# Metal Additive Manufacturing: A Review of Mechanical Properties

John J. Lewandowski and Mohsen Seifi

Department of Materials Science and Engineering, Case Western Reserve University (CWRU), Cleveland, Ohio 44106; email: JJL3@case.edu, mohsen.seifi@case.edu

**Keynote Topic**

This article is part of the **Materials Issues in Additive Manufacturing** keynote topic compilation.

Annu. Rev. Mater. Res. 2016. 46:151–86

First published online as a Review in Advance on April 21, 2016

The *Annual Review of Materials Research* is online at matsci.annualreviews.org

This article's doi: 10.1146/annurev-matsci-070115-032024



## Keywords

metal additive manufacturing, mechanical properties, fracture, fatigue, toughness, tensile

## Abstract

This article reviews published data on the mechanical properties of additively manufactured metallic materials. The additive manufacturing techniques utilized to generate samples covered in this review include powder bed fusion (e.g., EBM, SLM, DMLS) and directed energy deposition (e.g., LENS, EBF$^3$). Although only a limited number of metallic alloy systems are currently available for additive manufacturing (e.g., Ti-6Al-4V, TiAl, stainless steel, Inconel 625/718, and Al-Si-10Mg), the bulk of the published mechanical properties information has been generated on Ti-6Al-4V. However, summary tables for published mechanical properties and/or key figures are included for each of the alloys listed above, grouped by the additive technique used to generate the data. Published values for mechanical properties obtained from hardness, tension/compression, fracture toughness, fatigue crack growth, and high cycle fatigue are included for as-built, heat-treated, and/or HIP conditions, when available. The effects of test orientation/build direction on properties, when available, are also provided, along with discussion of the potential source(s) (e.g., texture, microstructure changes, defects) of anisotropy in properties. Recommendations for additional work are also provided.

## INTRODUCTION

A number of metal additive manufacturing (AM) processes are currently available (1), depending on the heat source (2, 3), such as electron beam (2–7), laser, or arc (2, 3, 8, 9), and on how the raw material is supplied. Materials supply can occur via powder or wire feed, whereby selected regions are melted at different combinations of absorbed power ($P$) and beam velocity ($V$) (10), as shown in **Figure 1**, and then solidified. Cooling rates during and after solidification are affected and controlled by the $P$-$V$ combinations utilized and by any preheating of the substrate. These variables, along with the subsequent thermal cycles that occur during such layered manufacturing as well as any postprocessing (e.g., heat treatment, HIP), affect the resulting microstructures, as reviewed previously (10) and in another contribution to this journal's keynote topic on AM (11). Nonequilibrium microstructures and defects can result in as-built materials, depending on the processing conditions and materials employed, whereas postprocessing via heat treatment and/or HIP can be used to change some of the microstructural features and to reduce or eliminate defects and any residual stresses. These changes affect both the orientation dependence of mechanical properties and their magnitude, as this article documents. A broader review on materials qualification needs for metal AM is provided elsewhere (10).

The recent reviews of the metal AM processes by Frazier (2) and Dutta & Froes (3) highlight some of the differences between the various processes. **Figure 2** provides the two major metal AM process categories reviewed in this article, powder bed fusion (PBF) and directed energy deposition (DED). **Figure 2** also includes designations for the technologies currently available within each major process category [e.g., direct metal laser melting (DMLM), selective laser melting (SLM), selective laser sintering (SLS), direct metal deposition (DMD)] and current commercial machine

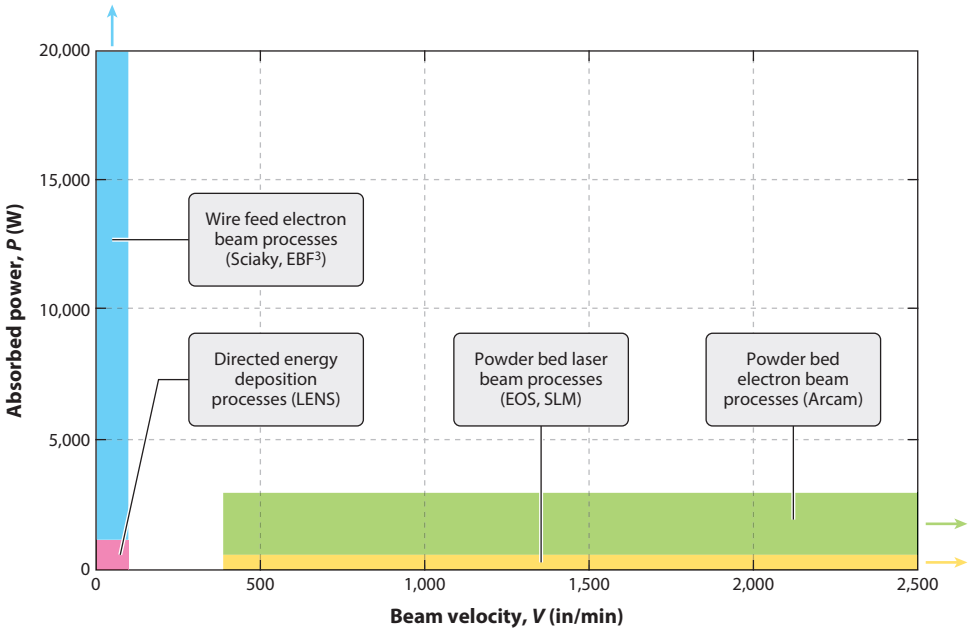


**Figure 1**

Typical combinations of power ($P$) and velocity ($V$) in various metal AM processes. Abbreviations: EBF$^3$, electron beam freeform fabrication; LENS, laser-engineered net shaping; SLM, selective laser melting. Adapted with permission from Reference 10.

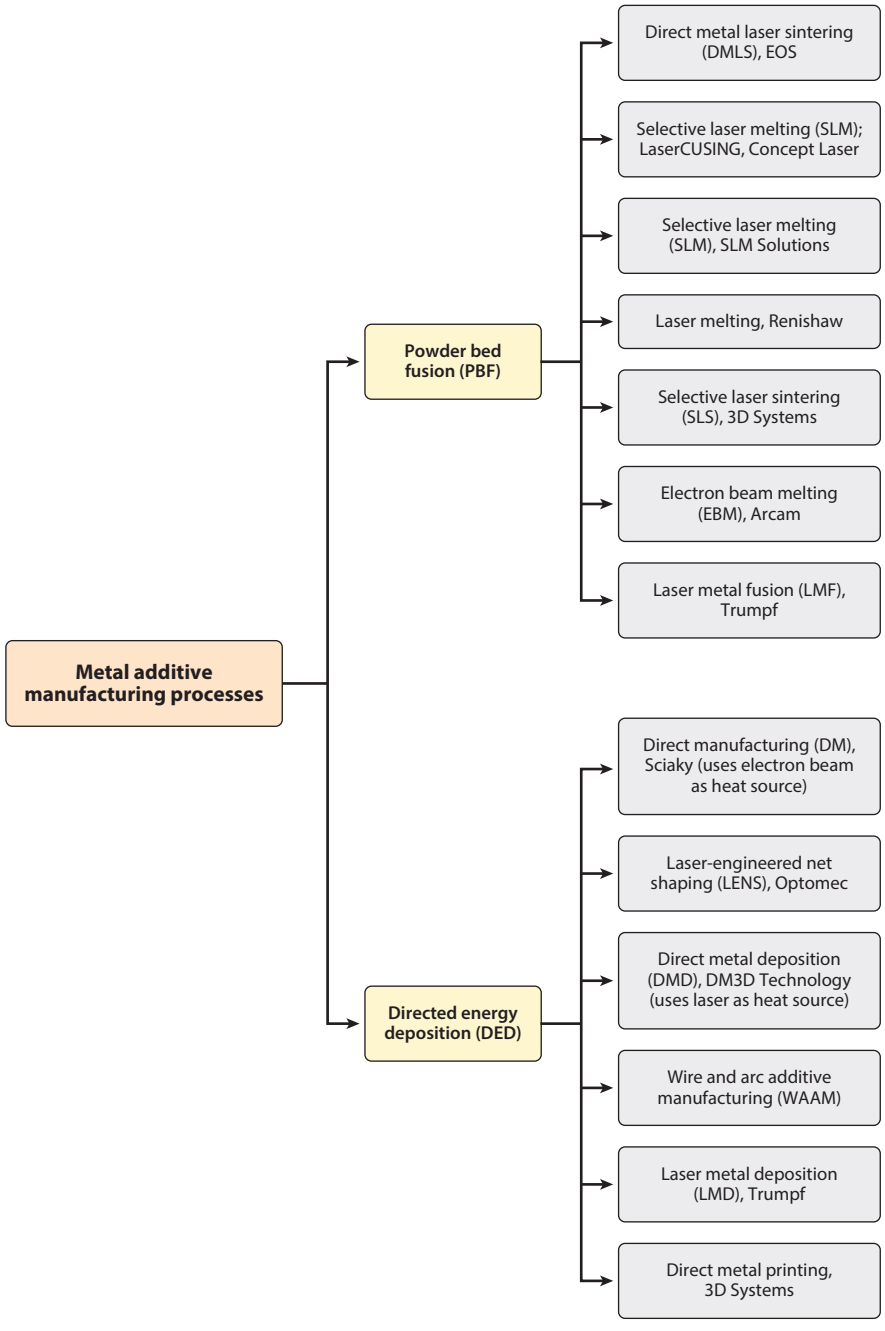


**Figure 2**

Summary of metal additive manufacturing processes, along with their commercial machine supplier names.

**Table 1 Summary of various alloys used in different process categories, along with references**

| | PBF | | DED | | | | |
|---|---|---|---|---|---|---|---|
| | EBM (powder) | Laser (powder) | EBM (wire; Sciaky) | EBM (powder) | Laser (wire) | Laser (powder; LENS) | WAAM (wire) |
| Titanium alloys | 12–48 | 49–71 | | | 72–79 | 80–83 | 74 |
| TiAl (intermetallics) | 199, 203–222 | 171, 172, 223, 224 | | | | | |
| Steel alloys | | 84–93 | 94 | | 95 | | 96 |
| Nickel alloys | 97–102 | 103–110 | | | 111, 112 | | |
| Aluminum alloys | | 113–124 | 125 | | | | 126, 127 |
| High-entropy alloys | 128 | 129 | | | | | |

suppliers. To systematically review the published values for mechanical properties obtained for materials manufactured by these different techniques, this review begins with a compilation of the most widely utilized AM alloy systems along with the process category (e.g., PBF, DED) and energy source for fusion [e.g., electron beam melting (EBM), laser, and wire and arc additive manufacturing (WAAM)]. Individual tables and/or figures for each alloy, energy source, and/or mechanical property are then provided for as-built, heat-treated, and/or HIP conditions and document the test orientation and build direction when available.

## ADDITIVELY MANUFACTURED ALLOY SYSTEMS

As indicated in previous reviews (2, 3), at present there is only a limited number of alloy systems for which mechanical properties are published. **Table 1** summarizes the existing alloy classes and references to published data, along with the process category and source of fusion. These categories provide the basis for the remainder of this review.

## MECHANICAL PROPERTIES OF ADDITIVELY MANUFACTURED METALLIC MATERIALS

Although most of the published mechanical property measurements have been reported for Ti-6Al-4V, tables and/or figures summarizing data for each of the alloy classes shown in **Table 1** are provided, when available. Review of the literature also reveals that most of the published work has focused on tension/compression testing, with more recent work on fracture-critical properties. In the tables, the effects of specimen or build orientation on tensile properties are documented using the *X*, *Y*, *Z* designation according to the ASTM standard (130) shown in **Figure 3**, when documented in the published work. Rectangular and nonsymmetric test coupons thus require three letters (*X*, *Y*, *Z*) to provide a complete orientation designation. In this terminology, *Z* designates the build direction. The *X* axis is parallel to the front of the machine and is perpendicular to *Z*. The *Y* axis is perpendicular to both the *Z* and *X* axes, with a positive direction defined to make a right-hand set of coordinates. The first letter designates the axis parallel to the longest overall dimension. The second letter designates the second-longest overall dimension, followed by the third letter, which designates the third-longest overall dimension of the coupon. For example, a specimen with *XYZ* designation has its longest dimension parallel to *X*, its second-longest dimension parallel to *Y*, and its shortest overall dimension parallel to *Z*. **Figure 3** also illustrates that only one letter

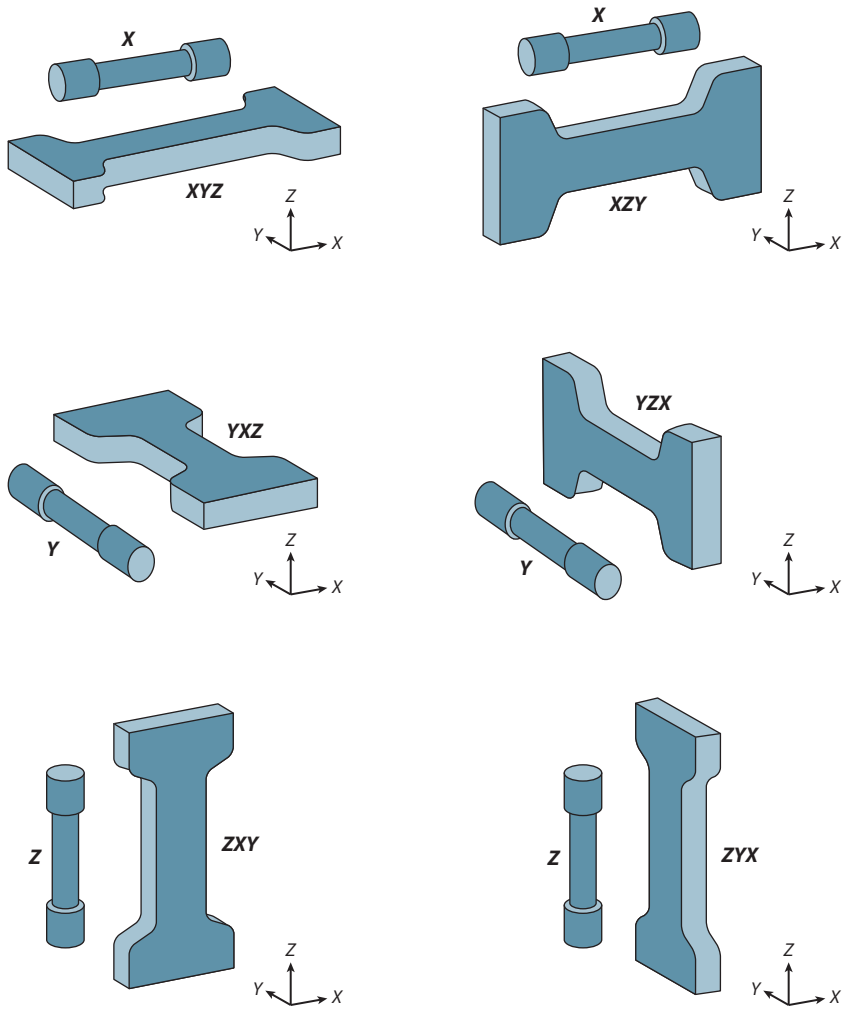


**Figure 3**

Orientation designations for mechanical testing of AM materials.

is required for cylindrically symmetric samples. Unfortunately, not all of the published works reviewed herein followed these ASTM/ISO rules. In some cases, only one letter was used for nonsymmetric samples. The tables also document any postprocessing (e.g., heat treatment, HIP) that was used.

ASTM committee F42 (131) is reviewing potential modifications to the orientation designation scheme for fracture toughness and fatigue crack growth, as shown in **Figure 4** (48). These modifications to the evolving ASTM standards for AM materials may be necessary to document the unique orientation- and location-dependent properties that can be produced both within and between builds in AM-processed materials (10, 48) due to differences in the microstructure, texture, residual stresses, and/or defects. These types of samples could also serve as witness samples deposited along with components in the same build to provide insight into part/component quality in different locations and orientations.

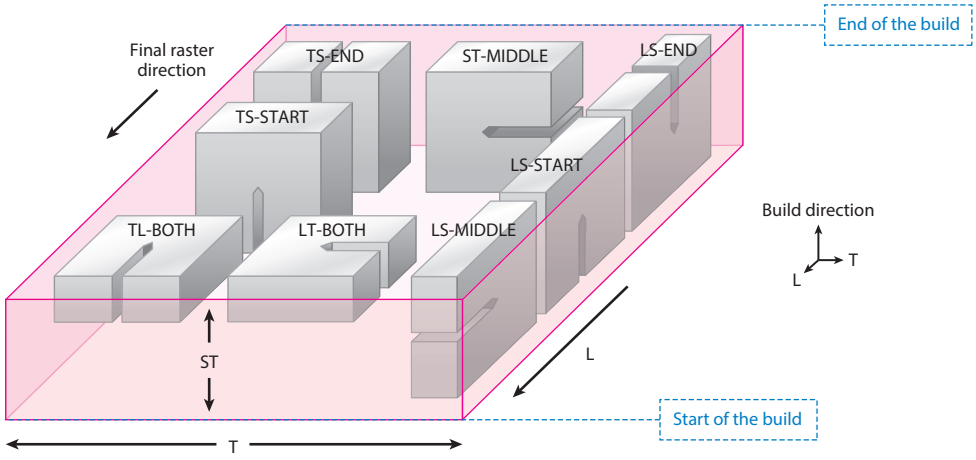


**Figure 4**

Possible designations for AM fracture and fatigue testing based on existing ASTM standards. There are eight different orientation and direction combinations. Abbreviations: L, longitudinal; S, short; T, transverse. Adapted from References 48 and 131 with permission.

## QUASI-STATIC PROPERTIES: TENSILE AND FRACTURE TOUGHNESS

**Tables 2** and **3** compile published tensile properties for Ti-6Al-4V produced via PBF EBM and laser techniques, respectively, and include hardness data when available along with literature references. In addition, **Tables 2** and **3** show the machine type and powder [e.g., conventional versus ELI (extra low interstitial)] utilized; show the specimen orientation using the *X*, *Y*, *Z* scheme presented in **Figure 3**; and specify whether the material was tested in the as-built, heat-treated, and/or HIP condition. **Figure 5** captures some of the key early observations on AM tensile properties for Ti-6Al-4V, and the tables and figures contained herein provide updated details along with many additional references.

The summary in **Table 2** for PBF (EBM) reveals orientation-dependent values for yield strength, ultimate tensile strength (UTS), and elongation to failure that are also affected by postprocessing heat treatments and/or HIP. Because of differences in the sample gauge lengths between the different investigations, the reported elongations to failure are difficult to compare directly. However, properties reported for all of the conditions (as built, heat treated, and/or HIP) often approach and exceed those reported for conventionally processed Ti-6Al-4V (3). EBM machine type (e.g., Arcam A1, A2, A2X, S12, S400) appears to affect the reported properties, although property variations have also been documented on samples manufactured within one machine type. The source(s) of these variations could be explored by conducting round robin activities like those organized by NIST/ASTM (132, 133) for PBF (laser), and the source(s) of the orientation-dependent properties is starting to receive additional attention from the AM community. Orientation-dependent differences in the microstructure, texture, and defects contribute to some of these tensile property differences but become more important in the fracture-critical properties (e.g., HCF, fatigue crack growth, fracture toughness) reviewed below. Postprocessing (e.g., heat treatment and/or HIP) can be used to produce more desirable microstructures and to reduce or eliminate process-induced defects [e.g., lack of fusion (LoF), isolated porosity] but affects the cost-effectiveness of the process. In general, the use of preheated powder beds in the EBM process reduces the cooling rate during and after the AM process, typically producing

**Table 2 Summary of EBM PBF AM Ti-6Al-4V tensile properties**

| Machine type | Condition | Specimen orientation | *E* (GPa) | Yield strength (MPa) | Ultimate tensile strength (MPa) | Elongation (%) | Hardness (Hv) | Reference |
|---|---|---|---|---|---|---|---|---|
| Arcam | Heat treated | *ZX* | NA | 869 ± 7 | 965 ± 5 | 6 ± 0 | NA | 141 |
| Arcam A1 | As built | *XY* | NA | 783 ± 15 | 833 ± 22 | 2.7 ± 0.4 | NA | 142 |
| | | *ZX* | | 812 ± 12 | 851 ± 19 | 3.6 ± 0.9 | | |
| Arcam | As built | *XY* | NA | 870 ± 8.1 | 971 ± 3.1 | 12.1 ± 0.9 | NA | 12 |
| | | *Z* | | 879 ± 12.5 | 953 ± 8.8 | 13.8 ± 0.9 | | |
| | HIP | *XY* | | 866 ± 6.4 | 959 ± 8.2 | 13.6 ± 0.6 | | |
| | | *Z* | | 868 ± 2.9 | 942 ± 2.6 | 12.9 ± 0.8 | | |
| Arcam ELI[a] | As built | *XY* | NA | 817 ± 4.3 | 918 ± 1.0 | 12.6 ± 0.8 | NA | |
| | | *Z* | | 802 ± 7.9 | 904 ± 6.0 | 13.8 ± 0.9 | | |
| | HIP | *XY* | | 814 ± 2.4 | 916 ± 2.5 | 13.6 ± 1.2 | | |
| | | *Z* | | 807 ± 8.4 | 902 ± 8.7 | 14.8 ± 0.5 | | |
| Arcam A2X ELI[a] | As built | *XY* | NA | 851.8 ± 5.8 | 964 ± 0.3 | 16.3 ± 0.8 | NA | 143 |
| Arcam A2 ELI[a] | As built | *Z* | NA | 928 ± 13.3 | 1,011 ± 14.8 | 13.6 ± 1.4 | NA | 31 |
| | HIP | *Z* | NA | 813 ± 14.3 | 908 ± 3.2 | 17.7 ± 0.9 | NA | |
| Arcam S12 | As built | *XY* | NA | 975 | 1,033 | 16.78 | NA | 144 |
| Arcam | As built | *XY* | NA | 881 ± 12.5 | 978 ± 11.5 | 10.7 ± 1.5 | NA | 33 |
| | HIP | *XY* | NA | 876 ± 12.5 | 978 ± 9.5 | 13.5 ± 1.5 | NA | |
| Arcam S12 | As built | *XY* | NA | 982 ± 5.7 | 1,029 ± 7 | 12.2 ± 0.8 | 372 ± 7.2 | 145 |
| | | *Z* | NA | 984 ± 8.5 | 1,032 ± 12.9 | 9 ± 2.9 | 367 ± 8.3 | |
| Arcam S400 | As built | *XY* | NA | 899 ± 4.7 | 978 ± 3.2 | 9.5 ± 1.2 | NA | 39 |
| | | *ZX* | | 869 ± 7.2 | 928 ± 9.8 | 9.9 ± 1.7 | | |
| Arcam S400 | As built | *XY* | 104 ± 2.3 | 844 ± 21.6 | 917 ± 30.53 | 8.8 ± 1.42 | NA | 40 |
| | | *Z* | 101 ± 2.5 | 782 ± 5.1 | 842 ± 13.84 | 9.9 ± 1.02 | NA | |
| Arcam S400 ELI[a] | As built | *Z* | NA | 1,150 | 1,200 | 16 | 380 | 146 |
| Arcam | As built | NA | 118 ± 5 | 830 ± 5 | 915 ± 10 | 13.1 ± 0.4 | NA | 16 |
| | HIP | NA | 117 ± 4 | 795 ± 10 | 870 ± 10 | 13.7 ± 1 | NA | |
| Arcam A2 ELI[a] | As built | *Z* | 93 ± 2 | 735 ± 28 | 775 ± 26 | 2.3 ± 0.8 | 369 ± 2 | 29 |

(*Continued*)

**Table 2** (*Continued*)

| Machine type | Condition | Specimen orientation | *E* (GPa) | Yield strength (MPa) | Ultimate tensile strength (MPa) | Elongation (%) | Hardness (Hv) | Reference |
|---|---|---|---|---|---|---|---|---|
| Arcam ELI[a] | HIP | *XY* | NA | 841 | 938 | 20 | NA | 14 |
| | As built | *Z* | NA | 856 | 924 | 15 | NA | |
| | HIP | *Z* | NA | 800 | 876 | 16 | NA | |
| Arcam | As built | NA | 114 ± 6 | 1,135 ± 12 | NA | NA | NA | 147 |
| Arcam S400 | As built | *Z* | 109 ± 2.1 | 1,098 ± 15 | 1,237 ± 13 | 8.8 ± 0.6 | NA | 148 |
| Arcam | As built | NA | 128 | 880 | 930 | >10% | NA | 149 |

NA denotes data not available.
[a]ELI (extra low interstitial) powder was used.

$\alpha + \beta$ lamellar microstructures [with prior $\beta$ grain sizes that can be affected or controlled by the combinations of *P* and *V* utilized in the process (134–140)]. EBM AM materials typically possess lower levels of residual stresses in the as-built condition than do materials made by laser-based techniques that typically use no preheat; the faster cooling rates typically produce highly nonequilibrium microstructures [e.g., martensite in PBF (laser) Ti-6Al-4V] and much higher levels of residual stress that require subsequent stress relief treatments, as described below. Chemistry control in the PBF (EBM) process can also become an issue in Ti-6Al-4V due to the preferential loss of Al during EBM of powders in high vacuum.

**Table 3** illustrates that PBF (laser) of Ti-6Al-4V exhibited features (e.g. orientation-dependent properties, machine effects (132, 133), postprocessing improvements to properties) similar to those shown for PBF (EBM) in **Table 2**. Highly nonequilibrium microstructures (e.g., martensite), along with substantial residual stresses that increase the strength and decrease the elongation values, are possible in as-built Ti-6Al-4V. Postprocessing has been used to increase the elongation to failure while reducing the yield strength, UTS, and residual stress values.

**Table 4**, which summarizes DED (laser) tensile properties, shows similar general characteristics of orientation- and machine-dependent properties, with values for as-built yield strength, UTS, and elongation to failure generally between the values exhibited in **Tables 2** and **3** for PBF (EBM) and PBF (laser), respectively. The combinations of *P* and *V* shown in **Figure 1** for DED generally produce $\alpha + \beta$ lamellar microstructures, with prior $\beta$ grain sizes somewhat larger than those obtained from PBF (laser) due to the slower cooling rates typically present in DED (57, 59, 134–137). **Table 4** also shows that HIP can result in significant increases to the elongation-to-failure values via the elimination of process-induced defects. These process-induced defects are particularly detrimental to the high cycle fatigue behavior, as discussed below.

**Table 5** summarizes the more limited published work on tensile properties for all of the other alloys in **Table 1** manufactured using PBF techniques. The limited published tensile properties for 316L PBF (laser) reveal properties in the range of commercially produced 316L. HIP of 316L produced via SLM increased elongation, likely due to the elimination of process-induced defects. Both Al-12Si and Al-Si-10Mg are alloys typically processed via commercial casting techniques (e.g., sand, gravity die). Strength levels in PBF (laser)–processed versions of Al-12Si and Al-Si-10Mg are in the range of data produced via sand and die casting techniques, whereas the somewhat higher elongation values arise due to the microstructure refinement provided by the faster cooling

**Table 3 Summary of laser-melted PBF AM Ti-6Al-4V tensile properties**

| Machine type | Condition | Specimen orientation | *E* (GPa) | Yield strength (MPa) | Ultimate tensile strength (MPa) | Elongation (%) | Hardness | Reference |
|---|---|---|---|---|---|---|---|---|
| EOS | As built | *XZY* | 91.8 ± 0.5 | 938 ± 7.7 | 1,140 ± 5 | NA | NA | 150 |
| | Stress relieved | | 98.2 ± 1.2 | 862 ± 3.1 | 936 ± 3.6 | | | |
| | HIP | | 106.8 ± 1.3 | 835 ± 3.8 | 910 ± 2.9 | | | |
| SLM | As built | *XY* | NA | 1,093 ± 64 | 1,279 ± 13 | 6 ± 0.7 | NA | 151 |
| | | *ZX* | | 1,125 ± 22 | 1,216 ± 8 | 6 ± 0.4 | | |
| | Stress relieved | *XY* | | 1,145 ± 17 | 1,187 ± 10 | 7 ± 2.7 | | |
| | | *ZX* | | 1,132 ± 13 | 1,156 ± 13 | 8 ± 0.4 | | |
| | Heat treated | *XY* | | 973 ± 8 | 996 ± 10 | 3 ± 0.4 | | |
| | | *ZX* | | 964 ± 7 | 998 ± 14 | 6 ± 2 | | |
| EOS M280 | As built | *ZX* | NA | 1,017 ± 7 | 1,096 ± 7 | 12 ± 0.5 | NA | 141 |
| SLM | As built | NA | 110 | 736 | 1,051 | 11.9 | 360 (Hv) | 152 |
| | HIP | | 115.4 | 885 | 973 | 19 | 351 (Hv) | |
| | Heat treated | | 117.4 | 1,051 | 1,115 | 11.3 | 321 (Hv) | |
| Renishaw MTT250 | As built | *XY* | NA | 910 ± 9.9 | 1,035 ± 29 | 3.3 ± 0.76 | NA | 153 |
| SLM250 | As built | *ZX* | NA | NA | 1,314 ± 15.6 | 4 ± 1.2 | NA | 154 |
| | HIP | | | | 1,088 ± 26.3 | 13.8 ± 1.3 | | |
| | Heat treated | | | | 1,228 ± 32.4 | 8 ± 15 | | |
| Renishaw AM250 | As built | *XZ* | 115 ± 6 | 978 ± 5 | 1,143 ± 6 | 11.8 ± 0.5 | NA | 155 |
| | | *ZX* | 119 ± 7 | 967 ± 10 | 117 ± 3 | 8.9 ± 0.4 | | |
| | | *XY* | 113 ± 5 | 1,075 ± 25 | 1,199 ± 49 | 7.6 ± 0.5 | | |
| | Stress relieved | *XZ* | 113 ± 9 | 958 ± 6 | 1,057 ± 8 | 12.4 ± 0.7 | | |
| | | *ZX* | 117 ± 6 | 937 ± 9 | 1,052 ± 11 | 9.6 ± 0.9 | | |
| | | *XY* | 112 ± 6 | 974 ± 7 | 1,065 ± 21 | 7.0 ± 0.5 | | |
| SLM250 | As built | *ZX* | NA | 1,008 | 1,080 | 1.6 | NA | 9 |
| | HIP | | | 962 | 1,080 | 5 | | |
| | Heat treated | | | 912 | 1,005 | 8.3 | | |
| Realizer | As built | *ZX* | 119 ± 7 | 967 ± 10 | 117 ± 3 | 8.9 ± 0.4 | NA | 64 |
| SLM50 | Stress relieved | | 117 ± 6 | 937 ± 9 | 1,052 ± 11 | 9.6 ± 0.9 | | |
| EOS M270 | As built | *ZX* | NA | 1,143 ± 30 | 1,219 ± 20 | 4.89 ± 0.6 | NA | 39 |
| | | *XY* | | 1,195 ± 19 | 1,269 ± 9 | 5 ± 0.5 | | |

(*Continued*)

**Table 3 (*Continued*)**

| Machine type | Condition | Specimen orientation | *E* (GPa) | Yield strength (MPa) | Ultimate tensile strength (MPa) | Elongation (%) | Hardness | Reference |
|---|---|---|---|---|---|---|---|---|
| SLM | As built | *XY* | 109.2 ± 3.1 | 1,110 ± 9 | 1,267 ± 5 | 7.28 ± 1.12 | NA | 156 |
| EOS M270 | As built | NA | 110 ± 5 | 990 ± 5 | 1,095 ± 10 | 8.1 ± 0.3 | NA | 51 |
| | Heat treated | | NA | 1,040 ± 10 | 1,140 ± 10 | 8.2 ± 0.3 | NA | |
| EOS M270 | As built | *ZX* | 111 | 1,120 | 1,257 | 8.0 | 37 (HRC) | 148 |
| EOS M27 | As built | *Z* | NA | 1,333 | 1,407 | 4.54 | NA | 157 |
| SLM (Trumpf) | As built | *XY* | 105 ± 5 | 1,137 ± 20 | 1,206 ± 8 | 7.6 ± 2 | NA | 158 |
| | | *ZX* | 102 ± 7 | 962 ± 47 | 1,166 ± 25 | 1.7 ± 0.3 | | |
| | Heat treated | *XY* | 103 ± 11 | 944 ± 8 | 1,036 ± 30 | 8.5 ± 1 | | |
| | | *ZX* | 98 ± 3 | 925 ± 14 | 1,040 ± 40 | 7.5 ± 2 | | |
| SLM | As built | NA | 94 | 1,125 | 1,250 | 6 | NA | 159 |
| Renishaw MTT | As built | *X* | NA | 1,166 ± 6 | 1,321 ± 6 | 2.0 ± 0.7 | NA | 160 |
| DLF | As built | *X* | 118 ± 2.3 | 1,100 ± 12 | 1,211 ± 31 | 6.5 ± 0.6 | NA | 161 |
| Concept Laser M2 | As built | *X* | NA | 1,070 ± 50 | 1,250 ± 50 | 5.5 ± 1 | NA | 162 |
| | | *Z* | | 1,050 ± 40 | 1,180 ± 30 | 8.5 ± 1.5 | | |

NA denotes data not available.

rates in the PBF (laser) processes used. The very limited published tension data on CoCrMo reveal that PBF (laser) exhibits somewhat higher strengths and lower elongation to failure than does PBF (EBM) in the as-built condition; these data also indicate orientation-dependent properties in the PBF (EBM) material. HIP and heat treatment of PBF (EBM) CoCrMo removed the orientation effects on properties and significantly increased the elongation to failure, consistent with HIP elimination of process-induced defects. There are not enough published data on the other alloy systems listed in **Table 5** to make sensible comparisons at this time.

**Table 6** summarizes the evolving database for DED, focusing on Inconel 718 (IN718). Properties are shown for both as-built and heat-treated conditions for a variety of machine types using either laser melting or EBM. Although there are not enough data reported within one machine type to make sensible comparisons, **Table 6** shows significant differences between the properties obtained on IN718 processed across the different machine types and energy sources used for melting.

Whereas there has been extensive research to determine the range of uniaxial tensile properties possible for PBF (EBM, laser) and DED (laser) reported in **Tables 2–6**, much less published research is available for the fracture-critical properties (e.g., toughness, fatigue) of Ti-6Al-4V, and very few published data exist for the fracture properties of the other alloy systems listed in **Table 1**. **Table 7** summarizes fracture toughness properties of Ti-6Al-4V for both PBF (laser)– and PBF (EBM)–processed materials, again using the *X*, *Y*, *Z* nomenclature shown in **Figure 3**. Candidate fracture toughness numbers, $K_q$, are provided in **Table 7** because thickness requirements for valid fracture toughness (i.e., $K_{Ic}$) measurements are not met in PBF (EBM) Ti-6Al-4V (48) and are not

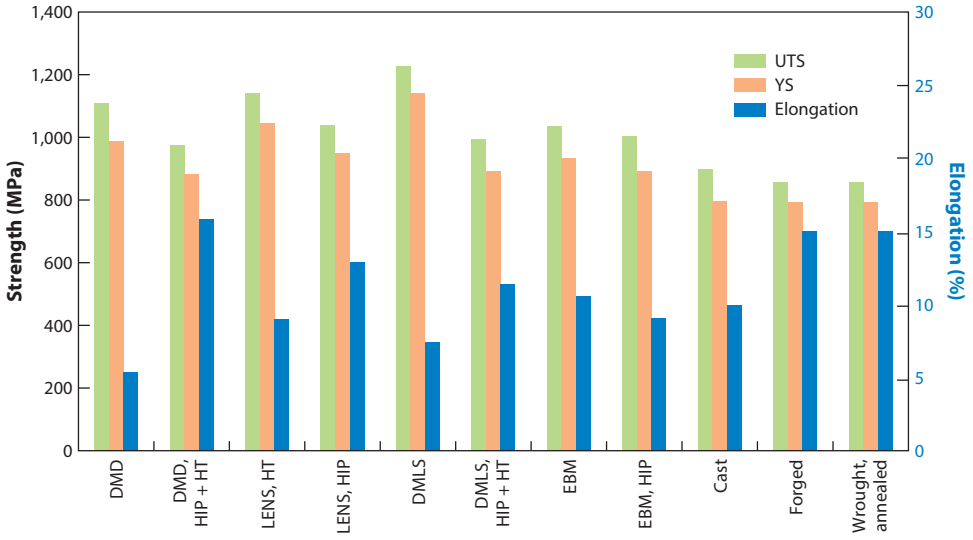


**Figure 5**

Summary of Ti-6Al-4V AM tensile properties. Abbreviations: DMD, direct metal deposition; DMLS, direct metal laser sintering; EBM, electron beam melting; HT, heat treated; LENS, laser-engineered net shaping; UTS, ultimate tensile strength; YS, yield stress. Adapted from Reference 3.

reported for PBF (laser) Ti-6Al-4V (151). Again, directly comparing toughness numbers between various works is difficult because few of the published values were obtained on samples sufficiently thick to provide valid $K_{Ic}$ (i.e., plane strain) measurements and because non–plane strain conditions (i.e., thinner samples) inflate toughness numbers due to plane stress conditions. Nonetheless, PBF (laser)–processed Ti-6Al-4V exhibits toughness values well below those of conventionally processed Ti-6Al-4V (48, 140, 196) and exhibits orientation-dependent values and significant effects of machine type and postprocessing conditions. In general, the as-built PBF (laser) Ti-6Al-4V exhibits the lowest toughness in the as-built condition, likely due to a combination of highly nonequilibrium microstructures, significant residual stresses, and process-induced defects. Stress relief, heat treatment, and/or HIP postprocessing appear to improve the toughness values reported in **Table 7** by reducing harmful residual stresses, by generating more favorable microstructures, and by minimizing defects in the as-built PBF (laser) material. The highest published toughness for the PBF (laser) Ti-6Al-4V reported in **Table 7** belongs to the EOS M280 processed material ($K_q = 86.3$ MPa$\sqrt{m}$) after a postprocessing heat treatment (194), whereas the as-built and/or HIP versions exhibited significantly lower toughness values.

In contrast, **Table 7** reveals significantly higher toughness values from preliminary studies on PBF (EBM) Ti-6Al-4V (48, 140) in both as-built and HIP-processed material, although machine-, orientation-, and location-dependent toughness values were exhibited. More recent work (10) suggested that both microstructure and texture variations and defect population vary with different build orientations, locations, and machines, thereby affecting the magnitude of toughness. **Figure 6** shows the fracture surface of an as-built PBF (EBM) Ti-6Al-4V toughness sample tested in the LT-BOTH orientation (10) shown in **Figure 4**. The various LoF defects that are evident perpendicular to the build direction in this LT-BOTH sample likely contribute to the orientation-dependent toughness values, although microstructural differences along and perpendicular to the build can also contribute (10), as suggested in **Figure 7**.

**Table 4 Summary of laser-fusion DED AM Ti-6Al-4V tensile properties**

| Machine type | Condition | Specimen orientation | *E* (GPa) | Yield strength (MPa) | Ultimate tensile strength (MPa) | Elongation (%) | Hardness | Reference |
|---|---|---|---|---|---|---|---|---|
| LENS (Optomec) | Stress relieved | *X* | 116 | 1,065 | 1,109 | 4.9 | NA | 58 |
| | | *Y* | 116 | 1,066 | 1,112 | 5.5 | | |
| | | *Z* | 112 | 832 | 832 | 0.8 | | |
| | HIP | *X* | 118 | 946 | 1,005 | 13.1 | | |
| | | *Y* | 118 | 952 | 1,007 | 13.0 | | |
| | | *Z* | 114 | 899 | 1,002 | 11.8 | | |
| DLD (Trumpf) | As built | *X* | NA | 950 ± 2 | 1,025 ± 10 | 12 ± 1 | NA | 72 |
| | | *Z* | | 950 ± 2 | 1,025 ± 2 | 5 ± 1 | | |
| | HIP | NA | | 850 ± 2 | 920 ± 1 | 17 ± 2 | | |
| LMD | As built | *X* | NA | 976 ± 24 | 1,099 ± 2 | 4.9 ± 0.1 | NA | 163 |
| LSF | As built | *Z* | NA | 1,070 | 1,140 | 6 | NA | 164 |
| LF[3] | As built | *X* | NA | 892 ± 10 | 911 ± 10 | 6.4 ± 0.6 | NA | 165 |
| | As built | *Z* | | 522 | 797 ± 27 | 1.7 ± 0.3 | | |
| | As built (machined) | *X* | | 984 ± 25 | 1,069 ± 19 | 5.4 ± 1 | | |
| | As built (machined) | *Z* | | 958 ± 14 | 1,026 ± 17 | 3.8 ± 0.9 | | |
| | Heat treated | *X* | | 681 ± 35 | 750 ± 20 | 4.8 ± 1.6 | | |
| | Heat treated | *Z* | | 637 ± 13 | 717 ± 12 | 3.4 ± 1.0 | | |
| | Heat treated (machined) | *X* | | 870 ± 37 | 953 ± 18 | 11.8 ± 1.3 | | |
| | Heat treated (machined) | *Z* | | 930 ± 15 | 942 ± 13 | 9.7 ± 2.2 | | |
| DMD | As built | *X* | NA | 1,105 ± 19 | 1,163 ± 22 | 4 ± 1 | NA | 166 |
| | Heat treated | *X* | | 975 ± 15 | 1,053 ± 18 | 7.5 ± 1 | | |
| IPG YLR | As built | *X* | NA | 960 ± 26 | 1,063 ± 20 | 10.9 ± 1.4 | NA | 80 |
| | | *Z* | | 958 ± 19 | 1,064 ± 26 | 14 ± 1 | | |

(*Continued*)

**Table 4** (*Continued*)

| Machine type | Condition | Specimen orientation | *E* (GPa) | Yield strength (MPa) | Ultimate tensile strength (MPa) | Elongation (%) | Hardness | Reference |
|---|---|---|---|---|---|---|---|---|
| LENS (Optomec) | As built (low power) | *X* | NA | 1,005 | 1,103 | 4 | NA | 167 |
| | Heat treated (low power) | | | 1,000 | 1,073 | 9 | | |
| | As built (high power) | | | 990 | 1,042 | 7 | | |
| | Heat treated (high power) | | | 991 | 1,044 | 10 | | |
| Laser forming | Heat treated | NA | NA | 839 | 900 | 12.3 | NA | 168 |
| DLF | Heat treated | NA | NA | 958 | 1,027 | 6.2 | NA | 169 |
| LENS | Heat treated | NA | NA | 827–965 | 896–1,000 | 1–16 | NA | 170 |
| LENS | As built | *Z* | 119 | 908 | 1,038 | 3.8 | NA | 226 |
| | Annealed | | 112 | 959 | 1,049 | 3.7 | | |
| | Heat treated | | 118 | 957 | 1,097 | 3.4 | | |

NA denotes data not available. Other abbreviations: DLD, direct laser fabrication; DMD, direct metal deposition; LMD, laser metal deposition; LSF, laser solid forming; $LF^3$, laser freeform fabrication.

**Figure 8** shows μCT analyses revealing process-induced defects in a large (i.e., 10 × 20 × 100 mm) as-built PBF (EBM) LT-BOTH Ti-6Al-4V fracture toughness sample that was tested to failure. Interestingly, although μCT analyses showed that HIP minimized or eliminated the defects present in **Figure 8**, **Table 7** and recently published work (10) report lower toughness values for HIP PBF (EBM) Ti-6Al-4V in comparison to the as-built material. Ongoing work is examining the details of the crack path and microstructure interactions to determine the source(s) of this reduction in toughness observed in the defect-free HIP versions (197).

The competition between microstructure-dominated (e.g., **Figure 7**) and defect-dominated (e.g., **Figures 6** and **8**) contributions to toughness may be responsible for these apparently conflicting observations in which defect-free PBF (EBM) HIP Ti-6Al-4V samples exhibit lower toughness than do their defect-containing as-built counterparts. **Figure 9** summarizes location-dependent toughness values along a tall, as-built PBF (EBM) Ti-6Al-4V sample, in addition to microstructure variations and significant differences in defect density along the build. Although HIP eliminates process-induced defects, location-dependent toughness values remain,

**Table 5 Summary of tensile properties of all other alloys listed in Table 2 and additively manufactured using PBF**

| Machine type | Alloy | Condition | Specimen orientation | *E* (GPa) | Yield strength (MPa) | Ultimate tensile strength (MPa) | Elongation (%) | Hardness | Reference |
|---|---|---|---|---|---|---|---|---|---|
| SLM250$^{HL}$ | TNM (Ti-Al-Nb-Mo) | As built (compression) | NA | NA | 1,620–1,651 | 1,816–1,903 | NA | NA | 171 |
| | | Heat treated (compression) | | | 886–1,071 | 1,428–1,671 | | | |
| EBM | TiAl | Heat treated (compression) | | 54 | 544 | 1,800 | 40 | NA | 172 |
| SLM | 316L | As built | NA | NA | NA | 600.2 ± 2.2 | 55 ± 2.5 | NA | 154 |
| | | Heat treated | | | | 617.9 ± 1.4 | 54.1 ± 1.6 | | |
| | | HIP | | | | 586.6 ± 2.4 | 64.4 ± 2.9 | | |
| SLM Concept Laser M1 | 316L | As built | NA | NA | 640 | 760 | 30 | NA | 173 |
| EOS M270 | 15-5 PH (precipitation-hardening stainless steel) | | | | 1,100 | 1,470 | 15 | | |
| EOS M250 | 4340 | Stress relieved | *XY* | 213.7 | 1,303 | 1,372 | 16–17 | 462–495 (Hv) | 86 |
| SLM250 Realizer | 316L | As built | *XY* | NA | 220–270 | 520–680 | 40–45 | NA | 93 |
| Arcam S12 | IN625 | As built | *Z* | NA | 410 | 750 | 44 | 14 (HRC) | 102 |
| | | HIP | | | 330 | 770 | 69 | 8 (HRC) | |
| EOS M280 | IN718 | Heat treated | *Z* | NA | 1,034 | 1,309 | 27 | NA | 105 |
| | | | *XY* | | 1,068 | 1,344 | 27 | | |
| SLM | IN718 | As built | *XY* | NA | 816 ± 24 | 1,085 ± 11 | 19.1 ± 0.7 | 35 (HRC) | 104 |
| | | | *Z* | | 737 ± 4 | 1,010 ± 10 | 20.6 ± 2.1 | 30 (HRC) | |
| | | Heat treated | *XY* | | 1,227 ± 1 | 1,447 ± 10 | 101 ± 0.6 | 45 (HRC) | |
| | | | *Z* | | 1,136 ± 16 | 1,357 ± 5 | 13.6 ± 0.2 | 45 (HRC) | |

| | | | | | | | | | |
|---|---|---|---|---|---|---|---|---|---|
| SLM | Al-Si-10Mg | As built | NA | 68 ± 3 | NA | 396 ± 8 | NA | 136 ± 9 (Hv) | 118 |
| | | Heat treated | | 66 ± 5 | | 399 ± 7 | | 152 ± 5 (Hv) | |
| SLM250 HL | Al-12Si | As built | NA | NA | 220.5 ± 9.4 | 418.9 ± 9.3 | 3.91 ± 0.3 | NA | 115 |
| | | Heat treated | | | 202.2 ± 4.3 | 369.3 ± 3.4 | 4.38 ± 0.16 | | |
| SLM | Al-12Si | As built | NA | NA | 223.5 | 355.1 | 4.2 | NA | 174 |
| SLM | Al-Si-10Mg | As built | *Z* | 70.7 ± 1.3 | 168.8 ± 1.3 | 272.8 ± 2.9 | 8.2 ± 0.3 | NA | 124 |
| | | | *XY* | 70.2 ± 1.2 | 169 ± 1 | 267 | 9.1 ± 0.5 | | |
| SLM | Al-Si-10Mg | As built | NA | NA | 207.8 | 367.7 | 4 | NA | 174 |
| SLM | Al-12Si | As built | *XY* | NA | 224 ± 7 | 368 ± 11 | 4.8 ± 0.6 | NA | 175 |
| SLM100 Realizer | Al-12Si | As built | *XY* | NA | 240 | 360 | 4 | NA | 176 |
| | | Heat treated | | | 110 | 190 | 5 | | |
| SLM Concept Laser M2 | Al-Si-10Mg | As built | *XY* | NA | ~250 | ~330 | ~1.2 | NA | 177 |
| | | | *Z* | | ~240 | ~320 | ~1 | | |
| EOS M270 | Al-Si-10Mg | As built | *XY* | 73 ± 1 | 243 ± 7 | 330 ± 3 | 6.2 ± 0.3 | 105 ± 2 (Hv) | 178 |
| | | | *Z* | 72 ± 1 | 231 ± 3 | 329 ± 2 | 4.1 ± 0.2 | 108 ± 3 (Hv) | |
| SLM Concept Laser M1 | Al-Si-10Mg | As built | *XY* | 68 ± 3 | NA | 391 ± 6 | 5.55 ± 0.4 | 127 (HV) | 179 |
| | | | *Z* | | | 398 ± 8 | 3.47 ± 0.6 | | |
| SLM | CoCrMo | As built | *XY* | NA | 738 ± 9.9 | 1,050 ± 12.2 | 5.2 ± 0.3 | 39.7 ± 1.2 (HRC) | 180 |
| | | | *Z* | | 685.3 ± 10.5 | 970 ± 9.8 | 3.9 ± 0.2 | 34.3 ± 1.2 | |
| EBM | CoCrMo | As built | *XY* | NA | 717 | 1,110 | 5 | NA | 181 |
| | | | *Z* | | 786 | 869 | 0.8 | | |
| | | HIP +heat treated | *XY* | | 586 | 1,145 | 30 | | |
| | | | *Z* | | 586 | 1,151 | 30 | | |
| SLM | CoCrMo | As built | NA | NA | 1,050 ± 150 | 1,300 ± 150 | >6 | 42 ± 4 (HRC) | 182 |
| EBM | Niobium | As built | *Z* | NA | 141 | 225 | 34.25 | NA | 183 |
| SLM | AZ91D | As built | *XY* | NA | 254 | 296 | ~1 | 100 (Hv) | 184 |

NA denotes data not available.

**Table 6 Summary of tensile properties of other alloys additively manufactured by DED**

| Machine type | Alloy | Condition (as built, HIP, or heat treated) | Specimen orientation | *E* (GPa) | Yield strength (MPa) | Ultimate tensile strength (MPa) | Elongation (%) | Hardness | Reference |
|---|---|---|---|---|---|---|---|---|---|
| GTAW | TiAl | As built | *Y* | NA | 474 ± 17 | 549 ± 23 | 0.5 | NA | 185 |
| | | | *Z* | | 424 ± 30 | 488 ± 50 | 0.5 | | |
| DMD | 4340 | Stress relieved | *XY* | NA | 1,398.65 | NA | 1.665 | NA | 95 |
| DLD (LENS) | 316L | As built | *Z* | NA | 405–415 | 620–660 | 34–40 | NA | 225 |
| | | Heat treated | *Z* | NA | 325–355 | 600–620 | 42–43 | NA | |
| SMD | IN718 | As built | *XY* | NA | 473 ± 6 | 828 ± 8 | 28 ± 2 | NA | 186 |
| DLD | IN718 | As built | *Z* | NA | 650 | 1,000 | NA | NA | 187 |
| | | Heat treated | | | 1,257 | 1,436 | | | |
| Laser | IN718 | As built | NA | NA | 590 | 845 | 11 | NA | 188 |
| | | Heat treated | | | 1,133 | 1,240 | 9 | | |
| EBF[3] | IN718 | As built | *XY* | 159 | 580 | 910 | 22 | NA | 189 |
| EBF[3] | IN718 | As built | *XY* | 138 | 655 | 978 | NA | NA | 99 |
| | | | *YX* | 194 | 699 | 936 | | | |
| | | Heat treated | *XY* | 174 | 986 | 1,114 | | | |
| | | | *YX* | 192 | 998 | 1,162 | | | |
| DLD | IN718 | Heat treated | NA | NA | 1,097.6 | 1,321 | 9.8 | NA | 111 |
| DLD | IN718 | Heat treated | NA | NA | 1,034 | 1,276 | 12 | NA | 190 |
| Laser/wire | IN718 | Heat treated | NA | NA | 1,079 | 1,314 | 20.4 | NA | 191 |
| WAAM | AA2319 | As built | *X* | NA | 114 ± 4.8 | 263 ± 0.5 | 18 ± 0.5 | NA | 127 |
| | | | *Y* | | 106 ± 0.8 | 258 ± 2.2 | 15.5 ± 1 | | |

NA denotes data not available.

suggesting that subtle detrimental changes to the microstructure may be responsible. More work is clearly needed to resolve these issues, and testing of much thicker samples is necessary to obtain valid $K_{Ic}$ measurements.

The relatively high toughness values obtained for the as-built PBF (EBM) Ti-6Al-4V shown in **Table 7** appear promising from a damage tolerance perspective. However, the presence of process-induced defects significantly reduces HCF properties, as discussed below.

**Table 8** provides $K_q$ toughness values for PBF (EBM) Ti-Al 4822 (198, 199) in both the as-built and HIP conditions. Although only very limited data exist, the toughness values were similar to those previously obtained for as-cast Ti-Al 4822 (200). However, the scale and homogeneity of the microstructures of the as-built and HIP PBF (EBM) TiAl were very different from one another and from those of the as-cast TiAl (200). The presence of process-induced defects in the

**Table 7 Summary of AM Ti-6Al-4V PBF (laser/EBM) fracture toughness**

| Process category | Machine type | Condition | Specimen orientation | Specimen type | $K_q$ (MPa$\sqrt{m}$) | Reference |
|---|---|---|---|---|---|---|
| **PBF(laser)** | SLM | As built | *XY* | CT | 28 ± 2 | 151 |
| | | | *XZ* | | 23 ± 1 | |
| | | | *ZX* | | 16 ± 1 | |
| | | Stress relieved | *XY* | | 28 ± 2 | |
| | | | *XZ* | | 30 ± 1 | |
| | | | *ZX* | | 31 ± 2 | |
| | | Heat treated | *XY* | | 41 ± 2 | |
| | | | *XZ* | | 49 ± 2 | |
| | | | *ZX* | | 49 ± 1 | |
| | SLM MTT250 | As built | *XY* | | 66.9 ± 2.6 | 192 |
| | | | *XZ* | | 64.8 ± 16.9 | |
| | | | *YZ* | | 41.8 ± 1.7 | |
| | SLM | As built | *ZX* | | 52.4 ± 3.48 | 193 |
| | EOS M280 | As built | *XY* | | 37.5 ± 5 | 194 |
| | | HIP | | | 57.8 ± 5 | |
| | | Heat treated | | | 86.3 | |
| **PBF(EBM)** | Arcam A1 | As built | *XY* | | 110 ± 8.9 | 142 |
| | | | *ZX* | | 102 ± 7.4 | |
| | Arcam | As built | *XY* | | 96.9 | 195 |
| | | | *ZX* | | 78.1 | |
| | | HIP | *XY* | | 99.0 | |
| | | | *ZX* | | 83.1 | |
| | Arcam A2 | As built | *XYZ* | 3PB | 68, 80 | 48 |
| | | | *XZY* | | 76 | |
| | | | *ZXY*: middle | | 65, 66 | |
| | | | *ZXY*: near start | | 79 | 140 |
| | | | *ZXY*: near end | | 100 | |

as-built PBF (EBM) TiAl was confirmed by μCT, and many of these defects were eliminated with HIP. This produced less scatter in the toughness data reported, again suggesting a competition between microstructure-dominated and defect-dominated contributions to toughness.

## HIGH CYCLE FATIGUE AND FATIGUE CRACK GROWTH

As discussed above, process-induced AM defects (e.g., **Figures 6**, **8**, and **9**) and microstructure variation/changes (e.g., **Figures 7** and **9**) can affect the tensile and toughness properties. However, such defects, along with surface roughness and residual stresses, can dominate the cyclic behavior,

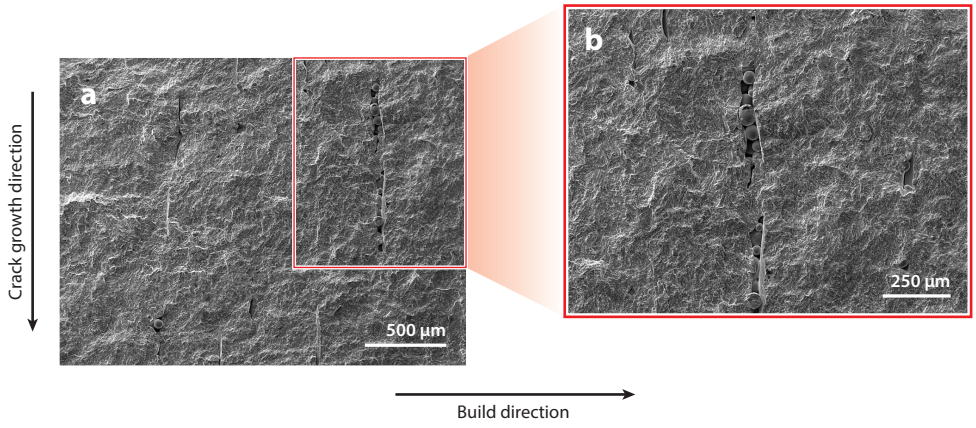


**Figure 6**

Lack-of-fusion (LoF) defects evident on the fracture surface of a PBF (EBM) as-built Ti-6Al-4V toughness sample tested in the LT-BOTH orientation shown in **Figure 4**. LoF defects are perpendicular to the build direction. (*a*) Low magnification. (*b*) Higher magnification.

can obscure microstructural effects, and can severely degrade the high cycle fatigue performance by providing potent fatigue initiation sites along with superimposed harmful residual stresses. These features can overwhelm any microstructural effects, as is shown below.

Although the early fatigue work of Kobryn & Semiatin (58) on LENS-processed (i.e., DED) Ti-6Al-4V exhibited HCF behavior that exceeded cast properties and was in the scatter band for cast + HIP and wrought-annealed Ti-6Al-4V (58), that work also revealed orientation-dependent fatigue life. More recent work (81) on LENS-processed Ti-6Al-4V documented defect-dominated fatigue behavior with fracture initiation from surface cracks and unmelted particles at the surface, as well as subsurface fatigue initiation from unmelted particles. Unmelted particles at the surface reduced the fatigue lifetime by an order of magnitude in comparison to subsurface crack initiation from unmelted particles in the bulk. However, when surface defects were suppressed by optimization

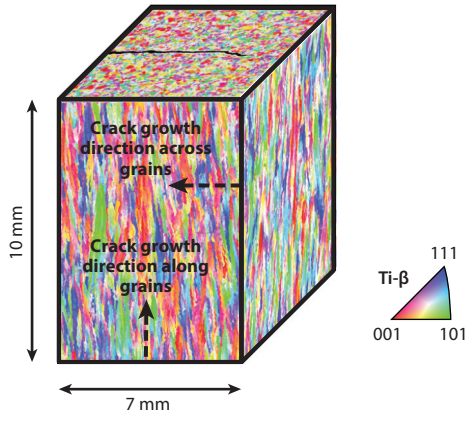


**Figure 7**

Large-area EBSD of an as-built PBF (EBM) Ti-6Al-4V sample showing crack growth across versus along reconstructed β grains. Adapted with permission from Reference 10.

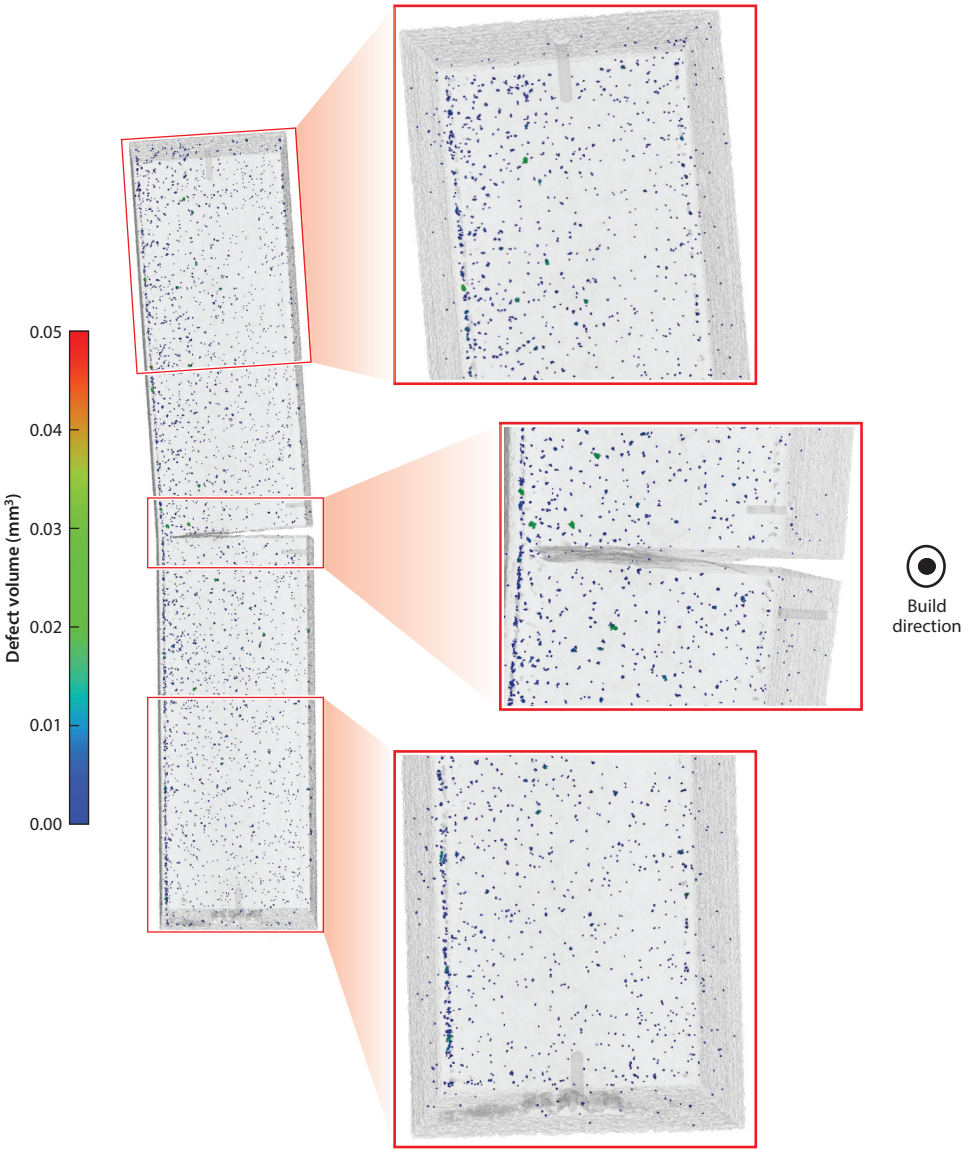


**Figure 8**

μCT images of a 10 × 20 × 100 mm as-built LT-BOTH PBF (EBM) Ti-6Al-4V toughness sample tested to failure in bending. Isolated defects (*dark spots*) are evident throughout the sample. Notch, fatigue precrack, cracked regions, and direct current potential drop lead holes are also shown. Build direction is out of page.

of the LENS process parameters (81), both as-deposited and simulated repair conditions could produce a fatigue life that exceeded the lower bound for wrought, annealed Ti-6Al-4V and that was in the upper-bound regions of cast + HIP material.

A very recent review (201) summarized the stress-controlled fatigue behavior of PBF (laser)–processed, PBF (EBM)–processed, and DED-processed Ti-6Al-4V, along with the effects of surface roughness (e.g., as built versus machined) and defects (e.g., as built versus HIP) in comparison

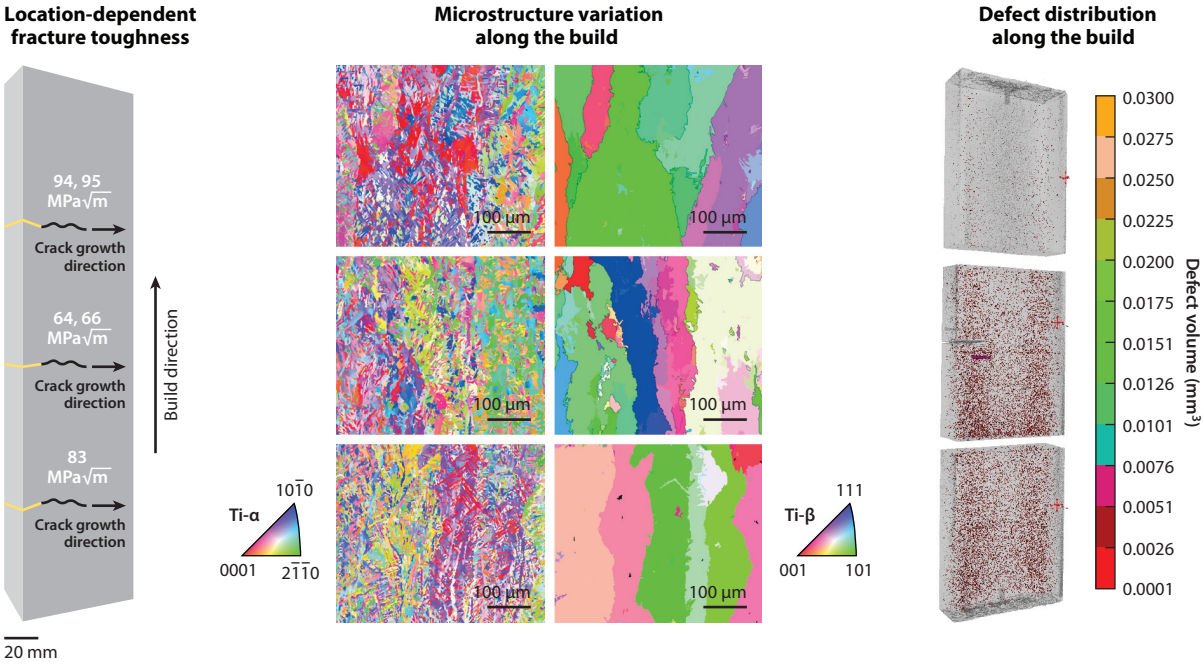


**Figure 9**

Illustration of location-dependent toughness values in an as-built PBF (EBM) Ti-6Al-4V sample. Variations in microstructure (prior β grains and $\alpha + \beta$ microstructure) and defect density were detected along the same as-built sample.

to as-cast and wrought Ti-6Al-4V tested with machined surfaces. **Figure 10** includes data from that work (201) in addition to a recent similar study on PBF (EBM) Ti-6Al-4V (202) conducted under strain control to capture the essence of the observations to date (201).

**Figure 10** shows summary data replotted (from Reference 201) of PBF (laser) *S-N* fatigue behavior for Ti-6Al-4V tested at $R = 0.1$, along with Metallic Materials Properties Development and Standardization (MMPDS) data obtained for cast (3-inch-thick) and wrought (annealed and aged) material with machined surfaces in addition to data obtained from Reference 202. Although orientation-dependent fatigue behavior was found and some property improvements were achieved with machined and polished surfaces, the very poor performance in comparison to the other data summarized in this plot was assumed to result from process-induced defects. Reference 201 indicates that the significantly improved fatigue data that were obtained by machining the as-built surfaces after optimization of the PBF (laser) process for Ti-6Al-4V support this hypothesis. However, this review (201) indicated that variations in laser process parameters created either a martensitic microstructure or a fine α microstructure. Fine α microstructure resulted in fatigue

**Table 8 Summary of AM γTi-Al 4822 fracture toughness for EBM PBF**

| Machine type | Alloy | Condition | Specimen orientation | Specimen type | $K_q$ (MPa$\sqrt{m}$) | Reference |
|---|---|---|---|---|---|---|
| Arcam A2X | Ti4822 | As built | *Z* | 3PB | 24.1 ± 6.5 | 198 |
| | | HIP | | | 27.8 ± 0.4 | |

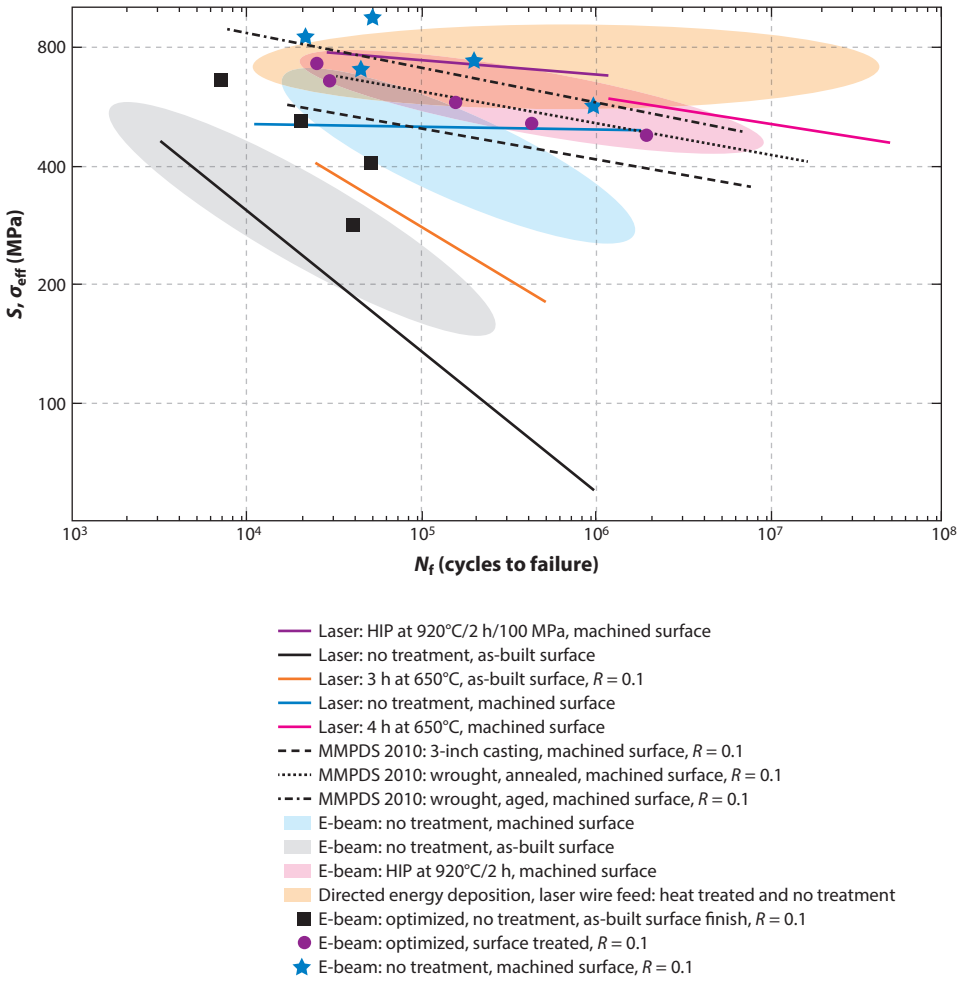


**Figure 10**

Summary of stress ($S$) versus cycles to failure ($N$) ($S$-$N$) data for PBF (laser), PBF (EBM), and wire (DED) at $R = 0.1$. Metallic Materials Properties Development and Standardization (MMPDS) data for cast, wrought machined data are shown for comparison. Data were obtained from a variety of sources, including References 12, 201, and 202. Adapted from Reference 201.

performance superior to that of MMPDS reference data for cast + HIP material, whereas the martensitic microstructure's performance was below that of the MMPDS reference data. Heat treatment at 650°C/3 h marginally improved fatigue behavior with the as-built rough surfaces, and cracking again appeared to initiate from the (rough) surfaces. Heat treatment at 650°C/4 h along with machined/EDM/shot-peened/sand-blasted surfaces produced fatigue performance that approached the fatigue performance of cast + HIP MMPDS data.

HIP of the PBF (laser) Ti-6Al-4V at 920°C/2 h/100 MPa, combined with surface machining, produced further improvements to the fatigue data in **Figure 10** via elimination of process-induced defects (201). However, although HIP at 1,050°C/4 h/100 MPa similarly eliminated process-induced defects, the associated microstructure coarsening at this HIP temperature reduced the fatigue performance. These results again emphasize the competition between defect-dominated

and microstructure-dominated contributions to properties. Although the presence of process-induced defects dominates high cycle fatigue performance and obscure microstructural effects, the removal of these defects via HIP or process optimization requires optimization of microstructural features to continue to improve performance.

**Figure 10** also includes data (from References 201 and 202) of PBF (EBM) and wire (DED) *S-N* fatigue behavior for Ti-6Al-4V tested at $R = 0.1$. The PBF (EBM)–processed samples tested with as-built (i.e., rough) surfaces reveals performance only slightly better than that of the worst-performing PBF (laser) samples shown. Some improvement in performance is provided by machining as-built surfaces (12), with more significant improvement reported recently on machined samples (202). However, the high cycle fatigue performance of the early work (12) on machined samples is well below that of the MMPDS cast Ti-6Al-4V data and is likely compromised by premature crack initiation at process-induced defects such as porosity. However, machining + HIP at 920°C/2 h/100 MPa (12) produced results comparable to MMPDS wrought data, again consistent with the HIP elimination of process-induced defects.

**Figure 10** also summarizes wire-fed DED fatigue performance. The good fatigue performance of DED-processed Ti-6Al-4V is attributed to the general lack of process-induced defects, whereas differences in the fatigue performance of the laser wire-fed and tungsten inert gas wire-fed Ti-6Al-4V were attributed to differences in microstructural scale (201).

**Table 9** summarizes the limited fatigue crack growth data reported for PBF (laser) and PBF (EBM) Ti-6Al-4V. Despite the generally low toughness values of the PBF (laser) Ti-6Al-4V summarized in **Table 7**, **Table 9** reveals Paris slope values at $R = 0.1$ in the range of 3–6, which is typical for metallic materials, and overload $K_c$ values in the range of the toughness values reported in **Table 7** for PBF (laser) Ti-6Al-4V. The higher-toughness PBF (EBM) Ti-6Al-4V exhibits much higher $K_c$ at overload in fatigue and similarly low Paris slope values and fatigue thresholds in the range of conventional Ti-6Al-4V. However, location- and orientation-dependent fatigue crack growth is evident in **Table 9** and is likely affected by the competition between microstructure-dependent and defect-dependent contributions to fatigue crack growth, which is somewhat similar to that proposed in **Figure 9** for toughness.

## CONCLUSIONS AND FUTURE RESEARCH PERSPECTIVE

**Figure 11** summarizes the range of mechanical properties typically generated in the mechanical characterization of metallic structural materials depending on their intended application. In that regard, this review summarizes published data currently available for AM metallic materials across the range of currently available PBF and DED process categories. Although the breadth of published mechanical properties has not covered the whole range of those shown in **Figure 11**, some of the mechanical properties reported for some of the metallic systems approach, and sometimes exceed, properties obtained on similar materials processed conventionally (e.g., casting, extrusion, forging). However, relatively few published data exist on standard samples, and little to no published work exists for low cycle fatigue, fatigue crack growth, fracture toughness, impact, creep, creep fatigue, multiaxial testing, or environmental effects. Furthermore, the current variability of properties (controlled by microstructure, residual stress, defects, etc.) within and between builds in one machine and across different machines and techniques, as well as the presence of process-induced defects and location/orientation-dependent properties, limits the more widespread use of these processing techniques for fracture-critical applications. The source(s), detection, and elimination of process-induced defects remain areas requiring additional focus to determine the microstructural features that will control properties with these processing techniques. These goals can be accomplished only by a better understanding of the fundamental

**Table 9 Summary of PBF AM Ti-6Al-4V fatigue crack growth properties**

| Process category | Condition | Specimen orientation | Specimen type | Load ratio ($R$) | $\Delta K_{th}$ (MPa$\sqrt{m}$) | Paris slope | $C$ (m/cycle) | $K_c$ (MPa$\sqrt{m}$) | Reference |
|---|---|---|---|---|---|---|---|---|---|
| **Laser melting** | As built | *XY* | CT (5 Hz) | 0.1 | NA | 3.37 | 5.79E-12 | NA | 151 |
| | | *XZ* | | | | 4.17 | 7.51E-12 | | |
| | | *ZX* | | | | 4.41 | 2.08E-12 | | |
| | Stress relieved | *XY* | | | | 5.84 | 9.93E-15 | | |
| | | *XZ* | | | | 3.24 | 1.16E-11 | | |
| | | *ZX* | | | | 3.35 | 8.85E-12 | | |
| | Heat treated | *XY* | | | | 3.83 | 2.04E-12 | | |
| | | *XZ* | | | | 3.11 | 1.71E-11 | | |
| | | *ZX* | | | | 2.94 | 2.58E-11 | | |
| | As built | *XY* | CT (10 Hz) | 0.1 | 6.3 ± 0.7 | 2.6 ± 0.3 | 1.2E-7 | 37 ± 4.3 | 192 |
| | | *XZ* | | | 5.8 ± 0.8 | 2.3 ± 0.3 | 5.8E-8 | 40 ± 25.1 | |
| | | *YZ* | | | 5.9 ± 1.0 | 2.4 ± 0.6 | 1.6E-7 | 37.11 ± 4 | |
| | As built | *ZX* | CT (10 Hz) | 0.1 | NA | 3.38 | 5E-12 | NA | 193 |
| **EBM** | As built | *XYZ* | 3PB (20 Hz) | 0.1 | 3.8 | 2.9 | NA | 91 | 140 |
| | | *XZY*: start | | | 5.7 | 4.1 | | 96 | |
| | | *XZY*: end | | | 4.2 | 3.5 | | 53 | |
| | | *XYZ* | | 0.3 | 3.8, 3.9 | 2.4, 2.3, 2.7 | | 83, 88, 96 | 48 |
| | | *XZY*: start | | 0.3 | 3.6 | 2.1 | | 87 | |
| | | *XZY*: end | | 0.3 | 4.9 | 2.4 | | 71 | |
| | | *ZXY*: middle | | 0.3 | 3.8 | 2.6 | | 69 | |
| | | *XYZ* | | 0.7 | 3.4 | 1.9 | | 78 | |
| | | *XZY*: start | | 0.7 | 3.5 | 1.4 | | 77 | |
| | | *XZY*: end | | 0.7 | 3.7 | 1.6 | | 63 | |

NA denotes data not available.

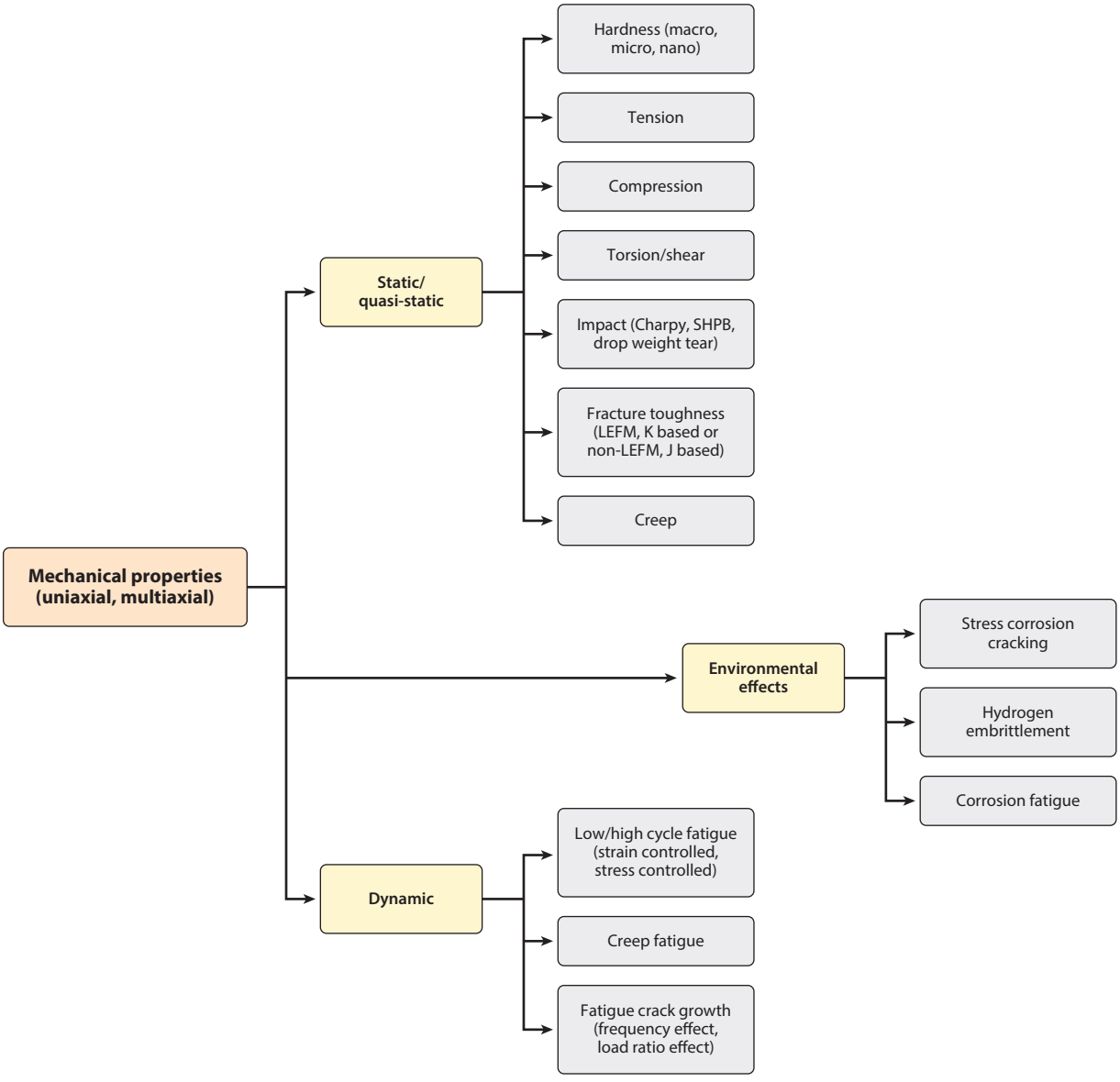


**Figure 11**

The range of mechanical properties typically generated for structural materials. The specific properties of interest depend on the intended application. Abbreviations: LEFM, linear elastic fracture mechanics; SHPB, split-Hopkinson pressure bar.

processing-structure-property relationships possible with this emerging technology. A more complete review of the evolving processing-microstructure-property relationships is in progress (203).

One approach that has recently been proposed (10) and that is summarized in **Figure 12** is to utilize Integrated Computation Materials (Science) and Engineering [ICM(S)E] to begin to address the multitude of issues that include development strategies for new alloys/microstructures

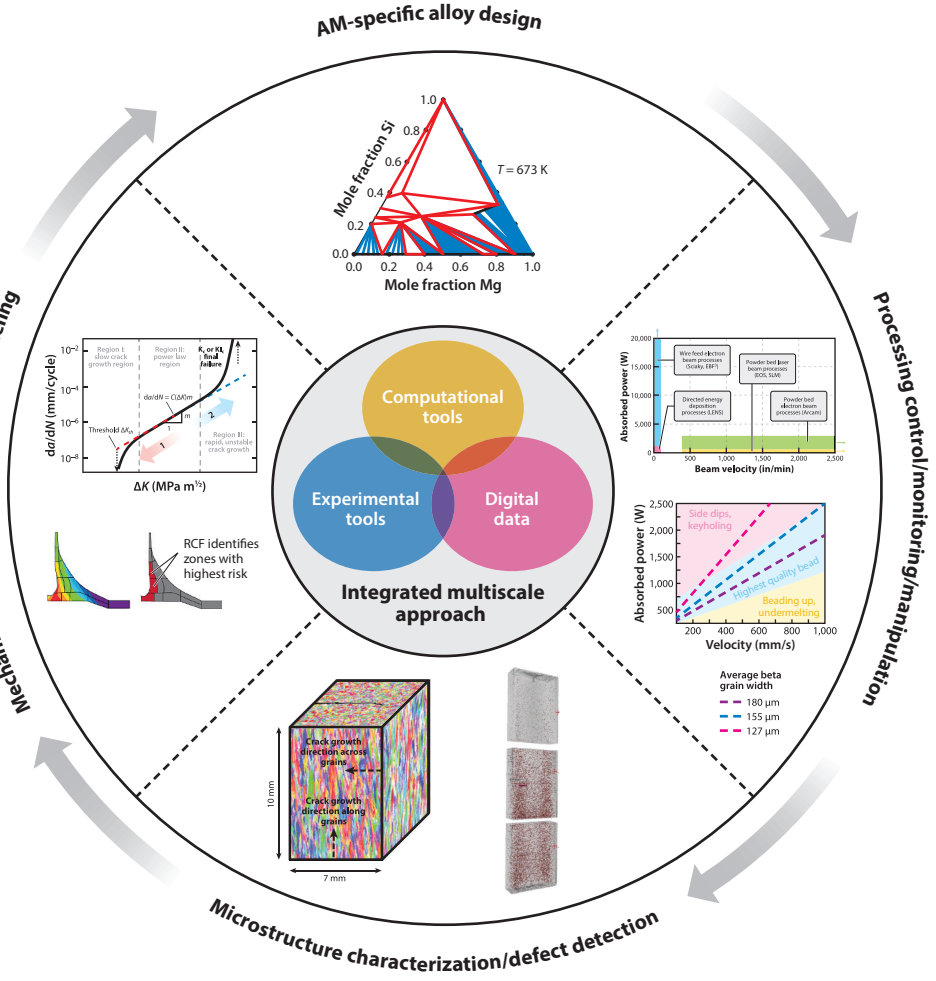


**Figure 12**

Integrated multiscale approach for the development of additively manufactured alloys for structural applications.

specifically designed to take advantage of AM as well as the lack of detailed process-structure-property understanding both within and across different machines that do not provide open source access. Some of the various challenges that have been summarized in more detail elsewhere (10) include lack of computationally efficient tools, lack of in situ commercial monitoring systems, lack of material/testing standards, feedstock and recyclability/reusability issues, surface roughness and residual stress management/control, process feedback and control, postprocessing via alternate heat treatments and/or HIP conditions, big data generation and handling issues, and probabilistic modeling of fracture-critical properties. Addressing these challenges in a cost-effective manner will require the integration of fundamental and applied approaches by various science and engineering disciplines at academic, industrial, and government institutions.

## DISCLOSURE STATEMENT

The authors are not aware of any affiliations, memberships, funding, or financial holdings that might be perceived as affecting the objectivity of this review.

## ACKNOWLEDGMENTS

The time spent gathering the information and generating some of the data reported in this article was partly supported by America Makes, the National Additive Manufacturing Innovation Institute, under project 4009, "Rapid Qualification Methods for Powder Bed Direct Metal Additive Manufacturing Processes," through contract FA8650-12-2-7230, and such support is highly appreciated. Additional support was provided by two ASTM International scholarship awards (M. Seifi) and by the Arthur P. Armington Professorship (J.J. Lewandowski). Mechanical testing and analyses at CWRU were conducted in the Advanced Manufacturing and Mechanical Reliability Center. M. Seifi appreciates various discussions with ASTM F42/E08/E07 committee members as well as significant interactions with YXLON, a division of Comet technologies, and GE inspection technologies regarding μCT results. The authors also appreciate fruitful collaboration with Materials Resources LLC for microstructural quantification/analyses.

## LITERATURE CITED

1. Kruth J-P, Leu MC, Nakagawa T. 1998. Progress in additive manufacturing and rapid prototyping. *CIRP Ann. Manuf. Technol.* 47(1):525–40
2. Frazier WE. 2014. Metal additive manufacturing: a review. *J. Mater. Eng. Perform.* 23(6):1917–28
3. Dutta B, Froes FHS. 2014. Additive manufacturing of titanium alloys. *Adv. Mater. Res.* 1019(Oct.):19–25
4. Facchini L, Magalini E, Robotti P, Molinari A. 2009. Microstructure and mechanical properties of Ti-6Al-4V produced by electron beam melting of pre-alloyed powders. *Rapid Prototyp. J.* 15(3):171–78
5. Parthasarathy J, Starly B, Raman S, Christensen A. 2010. Mechanical evaluation of porous titanium (Ti6Al4V) structures with electron beam melting (EBM). *J. Mech. Behav. Biomed. Mater.* 3(3):249–59
6. Murr LE, Gaytan SM, Ramirez DA, Martinez E, Hernandez J, et al. 2012. Metal fabrication by additive manufacturing using laser and electron beam melting technologies. *J. Mater. Sci. Technol.* 28(1):1–14
7. Collins PC, Haden CV, Ghamarian I, Hayes BJ, Ales T, et al. 2014. Progress toward an integration of process-structure-property-performance models for 'three-dimensional (3-D) printing' of titanium alloys. *JOM* 66(7):1299–309
8. Yu J, Rombouts M, Maes G, Motmans F. 2012. Material properties of Ti6Al4V parts produced by laser metal deposition. *Phys. Procedia* 39:416–24
9. Leuders S, Thöne M, Riemer A, Niendorf T, Tröster T, et al. 2013. On the mechanical behaviour of titanium alloy TiAl6V4 manufactured by selective laser melting: fatigue resistance and crack growth performance. *Int. J. Fatigue* 48:300–7
10. Seifi M, Salem A, Beuth J, Harrysson O, Lewandowski JJ. 2016. Overview of materials qualification need for metal additive manufacturing. *JOM* 68(3):747–64
11. Collins PC, Brice DA, Samimi P, Ghamarian I, Fraser HL. 2016. Microstructural control of additively manufactured materials. *Annu. Rev. Mater. Res.* 46:63–91
12. Ackelid U, Svensson M. 2009. Additive manufacturing of dense metal parts by electron beam melting. In *Proceedings of Materials Science and Technology Conference (MS&T)*, pp. 2711–19. Novelty, OH: ASM Int.
13. Chang Y, McLouth T, Pozuelo M, Chang C, Wooten J. 2015. The micro-mechanical behavior of electron beam melted Ti-6Al-4V alloy. In *TMS Proceedings*, pp. 211–18. Warrendale, PA/Hoboken, NJ: TMS/Wiley
14. Christensen A, Kircher R, Lippincott A. 2007. Qualification of electron beam melted (EBM) Ti6Al4V-ELI for orthopaedic applications. In *Proceedings from the Materials & Processes for Medical Devices Conference*, pp. 48–53. Novelty, OH: ASM Int.

15. Devika D, Dass SS, Kumar Chaudhary S. 2015. Characterization and corrosion behaviour study on biocompatible Ti-6Al-4V component fabricated by electron beam melting. *J. Biomimetics Biomater. Biomed. Eng.* 22:63–75
16. Facchini L, Magalini E, Robotti P, Molinari A. 2009. Microstructure and mechanical properties of Ti-6Al-4V produced by electron beam melting of pre-alloyed powders. *Rapid Prototyp. J.* 15(3):171–78
17. Gong H, Rafi K, Gu H, Starr T, Stucker B. 2014. Analysis of defect generation in Ti-6Al-4V parts made using powder bed fusion additive manufacturing processes. *Addit. Manuf.* 1–4:87–98
18. Gong X, Anderson T, Chou K. 2012. Review on powder-based electron beam additive manufacturing technology. In *Proceedings of the ASME International Symposium on Flexible Automation*, pp. 507–15. New York: ASME
19. Gong X, Lydon J, Cooper K, Chou K. 2013. Microstructural characterization and modeling of beam speed effects on Ti-6Al-4V by electron beam additive manufacturing. In *Solid Freeform Fabrication Proceedings*, pp. 459–69. Austin: Univ. Tex.
20. Gong X, Lydon J, Cooper K, Chou K. 2014. Beam speed effects on Ti-6Al-4V microstructures in electron beam additive manufacturing. *J. Mater. Res.* 29(17):1–9
21. Guo C, Ge W, Lin F. 2015. Effects of scanning parameters on material deposition during electron beam selective melting of Ti-6Al-4V powder. *J. Mater. Process. Technol.* 217:148–57
22. Hrabe N, Quinn T. 2013. Effects of processing on microstructure and mechanical properties of a titanium alloy (Ti-6Al-4V) fabricated using electron beam melting (EBM). Part 1. Distance from build plate and part size. *Mater. Sci. Eng. A* 573:264–70
23. Ikeo N, Ishimoto T, Serizawa A, Nakano T. 2014. Control of mechanical properties of three-dimensional Ti-6Al-4V products fabricated by electron beam melting with unidirectional elongated pores. *Metall. Mater. Trans. A* 45(10):4293–301
24. Jamshidinia M, Kovacevic R. 2015. The influence of heat accumulation on the surface roughness in powder-bed additive manufacturing. *Surf. Topogr. Metrol. Prop.* 3(1):014003
25. Juechter V, Scharowsky T, Singer RF, Körner C. 2014. Processing window and evaporation phenomena for Ti-6Al-4V produced by selective electron beam melting. *Acta Mater.* 76:252–58
26. Kalinyuk AN, Trigub NP, Semiatin SL. 2003. Microstructure, texture, and mechanical properties of electron-beam melted Ti-6Al-4V. *Mater. Sci. Eng. A* 346:178–88
27. Karlsson J, Norell M, Ackelid U, Engqvist H, Lausmaa J. 2015. Surface oxidation behavior of Ti-6Al-4V manufactured by Electron Beam Melting (EBM®). *J. Manuf. Process.* 17:120–26
28. Koike M, Greer P, Owen K, Lilly G, Murr LE, et al. 2011. Evaluation of titanium alloys fabricated using rapid prototyping technologies—electron beam melting and laser beam melting. *Materials* 4(12):1776–92
29. Koike M, Martinez K, Guo L, Chahine G, Kovacevic R, Okabe T. 2011. Evaluation of titanium alloy fabricated using electron beam melting system for dental applications. *J. Mater. Process. Technol.* 211(8):1400–8
30. Kok Y, Tan X, Tor S, Chua CK. 2015. Fabrication and microstructural characterisation of additive manufactured Ti-6Al-4V parts by electron beam melting. *Virtual Phys. Prototyp.* 10(1):13–21
31. Lu SL, Tang HP, Ning YP, Liu N, StJohn DH, Qian M. 2015. Microstructure and mechanical properties of long Ti-6Al-4V rods additively manufactured by selective electron beam melting out of a deep powder bed and the effect of subsequent hot isostatic pressing. *Metall. Mater. Trans. A* 46(9):3824–34
32. Markl M, Ammer R, Rüde U, Körner C. 2015. Numerical investigations on hatching process strategies for powder-bed-based additive manufacturing using an electron beam. *Int. J. Adv. Manuf. Technol.* 78(1–4):239–47
33. Mohammadhosseini A, Fraser D, Masood SH, Jahedi M. 2013. Microstructure and mechanical properties of Ti-6Al-4V manufactured by electron beam melting process. *Mater. Res. Innov.* 17(Suppl. 2):106–12
34. Murr LE. 2014. Metallurgy of additive manufacturing: examples from electron beam melting. *Addit. Manuf.* 5:40–53
35. Murr LE, Gaytan SM, Lopez MI, Martinez E, Medina F, Wicker RB. 2009. Metallographic characterization of additive-layer manufactured products by electron beam melting of Ti-6Al-4V powder. *Pract. Metallogr.* 46(9):442–53

36. Hrabe N, Kircher R, Quinn T. 2012. Effects of processing on microstructure and mechanical properties of Ti-6Al-4V fabricated using electron beam melting (EBM): orientation and location. In *Solid Freeform Fabrication Proceedings*, pp. 1045–58. Austin: Univ. Tex.
37. Ponader S, Vairaktaris E, Heinl P, Wilmowsky CV, Rottmair A, et al. 2008. Effects of topographical surface modifications of electron beam melted Ti-6Al-4V titanium on human fetal osteoblasts. *J. Biomed. Mater. Res. A* 84(4):1111–19
38. Puebla K. 2012. Effect of melt scan rate on microstructure and macrostructure for electron beam melting of Ti-6Al-4V. *Mater. Sci. Appl.* 3(5):259–64
39. Rafi HK, Karthik NV, Gong H, Starr TL, Stucker BE. 2013. Microstructures and mechanical properties of Ti6Al4V parts fabricated by selective laser melting and electron beam melting. *J. Mater. Eng. Perform.* 22(12):3872–83
40. Rafi K, Karthik N, Starr TL, Stucker BE. 2012. Mechanical property evaluation of Ti-6Al-4V parts made using electron beam melting. In *Solid Freeform Fabrication Proceedings*, pp. 526–35. Austin: Univ. Tex.
41. Safdar A, He HZ, Wei L-Y, Snis A, De Paz LEC. 2012. Effect of process parameters settings and thickness on surface roughness of EBM produced Ti-6Al-4V. *Rapid Prototyp. J.* 18(5):401–8
42. Safdar A, Wei L-Y, Snis A, Lai Z. 2012. Evaluation of microstructural development in electron beam melted Ti-6Al-4V. *Mater. Charact.* 65:8–15
43. Scharowsky T, Juechter V, Singer RF, Körner C. 2015. Influence of the scanning strategy on the microstructure and mechanical properties in selective electron beam melting of Ti-6Al-4V. *Adv. Eng. Mater.* 17(11):1573–78
44. Svensson M. 2013. Influence of interstitials on material properties of Ti-6Al-4V fabricated with Electron Beam Melting (EBM®). In *Proceedings from the Materials and Processes for Medical Devices Conference*, pp. 119–24. Novelty, OH: ASM Int.
45. Svensson M, Ackelid U, Ab A. 2010. Titanium alloys manufactured with electron beam melting mechanical and chemical properties. In *Proceedings of Materials & Processes for Medical Devices Conference*, pp. 189–94. Novelty, OH: ASM Int.
46. Wang X, Gong X, Chou K. 2015. Scanning speed effect on mechanical properties of Ti-6Al-4V alloy processed by electron beam additive manufacturing. *Procedia Manuf.* 1:287–95
47. Zhao H, Antonysamy AA, Meyer J, Ciuea O, Williams ST, Prangnell PB. 2015. Automated multi-scale microstructure heterogeneity analysis of selective electron beam melted Ti-6Al-4V components. In *TMS Proceedings*, pp. 429–36. Warrendale, PA/Hoboken, NJ: TMS/Wiley
48. Seifi M, Dahar M, Aman R, Harrysson O, Beuth J, Lewandowski JJ. 2015. Evaluation of orientation dependence of fracture toughness and fatigue crack propagation behavior of as-deposited ARCAM EBM Ti-6Al-4V. *JOM* 67(3):597–607
49. Behrendt U, Shellabear M. 1995. The EOS rapid prototyping concept. *Comput. Ind.* 28(1):57–61
50. Challis VJ, Xu X, Zhang LC, Roberts AP, Grotowski JF, Sercombe TB. 2014. High specific strength and stiffness structures produced using selective laser melting. *Mater. Des.* 63:783–88
51. Facchini L, Magalini E, Robotti P, Molinari A, Höges S, Wissenbach K. 2010. Ductility of a Ti-6Al-4V alloy produced by selective laser melting of prealloyed powders. *Rapid Prototyp. J.* 16(6):450–59
52. Fu CH, Guo YB. 2014. Three-dimensional temperature gradient mechanism in selective laser melting of Ti-6Al-4V. *J. Manuf. Sci. Eng.* 136(6):06 1004
53. Gong H, Gu H, Dilip JJS, Pal D, Stucker B, et al. 2014. Melt pool characterization for selective laser melting of Ti-6Al-4V pre-alloyed powder. In *Solid Freeform Fabrication Proceedings*. Austin: Univ. Tex.
54. Grimm T, Wiora G, Witt G. 2015. Characterization of typical surface effects in additive manufacturing with confocal microscopy. *Surf. Topogr. Metrol. Prop.* 3(1):014001
55. Hanzl P, Zetek M, Bakša T, Kroupa T. 2015. The influence of processing parameters on the mechanical properties of SLM parts. *Procedia Eng.* 100:1405–13
56. Khaing MW, Fuh JYH, Lu L. 2001. Direct metal laser sintering for rapid tooling: processing and characterisation of EOS parts. *J. Mater. Process. Technol.* 113(1–3):269–72
57. Kobryn PA, Semiatin SL. 2001. The laser additive manufacture of Ti-6Al-4V. *JOM* 53(9):40–42
58. Kobryn PA, Semiatin SL. 2001. Mechanical properties of laser-deposited Ti-6Al-4V. In *Solid Freeform Fabrication Proceedings*, pp. 179–86. Austin: Univ. Tex.

59. Kobryn P, Semiatin S. 2003. Microstructure and texture evolution during solidification processing of Ti-6Al-4V. *J. Mater. Process. Technol.* 135(2–3):330–39
60. Schnitzer M, Lisý M, Hudák R, Živ J. 2015. Experimental measuring of the roughness of test samples made using DMLS technology from the titanium alloy Ti-6Al-4V. In *IEEE International Symposium on Applied Machine Intelligence and Informatics, 13th*, pp. 31–36
61. Simchi A. 2006. Direct laser sintering of metal powders: mechanism, kinetics and microstructural features. *Mater. Sci. Eng. A* 428(1–2):148–58
62. Simchi A, Petzoldt F, Pohl H. 2003. On the development of direct metal laser sintering for rapid tooling. *J. Mater. Process. Technol.* 141(3):319–28
63. Simonelli M, Tse YY, Tuck C. 2012. Further understanding of Ti-6Al-4V selective laser melting using texture analysis. In *Solid Freeform Fabrication Proceedings*, pp. 480–91. Austin: Univ. Tex.
64. Simonelli M, Tse YY, Tuck C. 2014. The formation of $\alpha + \beta$ microstructure in as-fabricated selective laser melting of Ti-6Al-4V. *J. Mater. Res.* 29(17):2028–35
65. Thijs L, Verhaeghe F, Craeghs T, Van Humbeeck J, Kruth J-P. 2010. A study of the microstructural evolution during selective laser melting of Ti-6Al-4V. *Acta Mater.* 58(9):3303–12
66. Thombansen U, Abels P. 2015. Process observation in selective laser melting (SLM). *Proc. SPIE* 9356:93560R
67. Wauthle R, Vrancken B, Beynaerts B, Jorissen K, Schrooten J, et al. 2015. Effects of build orientation and heat treatment on the microstructure and mechanical properties of selective laser melted Ti6Al4V lattice structures. *Addit. Manuf.* 5:77–84
68. Wu X, Sharman R, Mei J, Voice W. 2004. Microstructure and properties of a laser fabricated burn-resistant Ti alloy. *Mater. Des.* 25(2):103–9
69. Wu X, Liang J, Mei J, Mitchell C, Goodwin PS, Voice W. 2004. Microstructures of laser-deposited Ti-6Al-4V. *Mater. Des.* 25(2):137–44
70. Xu W, Brandt M, Sun S, Elambasseril J, Liu Q, et al. 2015. Additive manufacturing of strong and ductile Ti-6Al-4V by selective laser melting via in situ martensite decomposition. *Acta Mater.* 85:74–84
71. 2001. EOS takes fine approach to laser sintering. *Met. Powder Rep.* 56(3):18
72. Qiu C, Ravi GA, Dance C, Ranson A, Dilworth S, Attallah MM. 2015. Fabrication of large Ti-6Al-4V structures by direct laser deposition. *J. Alloys Compd.* 629:351–61
73. Hofmann DC, Roberts S, Otis R, Kolodziejska J, Dillon RP, et al. 2014. Developing gradient metal alloys through radial deposition additive manufacturing. *Sci. Rep.* 4:5357
74. Wang F, Williams S, Colegrove P, Antonysamy AA. 2012. Microstructure and mechanical properties of wire and arc additive manufactured Ti-6Al-4V. *Metall. Mater. Trans. A* 44(2):968–77
75. Brandl E, Baufeld B, Leyens C, Gault R. 2010. Additive manufactured Ti-6A1-4V using welding wire: comparison of laser and arc beam deposition and evaluation with respect to aerospace material specifications. *Phys. Procedia* 5:595–606
76. Qian L, Mei J, Liang J, Wu X. 2005. Influence of position and laser power on thermal history and microstructure of direct laser fabricated Ti-6Al-4V samples. *Mater. Sci. Technol.* 21(5):597–605
77. Kobryn PA, Moore EH, Semiatin SL. 2000. Effect of laser power and traverse speed on microstructure, porosity, and build height in laser-deposited Ti-6Al-4V. *Scr. Mater.* 43(4):299–305
78. Brandl E, Leyens C, Palm F. 2011. Mechanical properties of additive manufactured Ti-6Al-4V using wire and powder based processes. *IOP Conf. Ser. Mater. Sci. Eng.* 26:012004
79. Kottman M, Zhang S, McGuffin-Cawley J, Denney P, Narayanan BK. 2015. Laser hot wire process: a novel process for near-net shape fabrication for high-throughput applications. *JOM* 67(3):622–28
80. Carroll BE, Palmer TA, Beese AM. 2015. Anisotropic tensile behavior of Ti-6Al-4V components fabricated with directed energy deposition additive manufacturing. *Acta Mater.* 87:309–20
81. Prabhu AW, Chaudhary A, Zhang W, Babu SS. 2015. Effect of microstructure and defects on fatigue behaviour of directed energy deposited Ti-6Al-4V. *Sci. Technol. Weld. Join.* 20(8):659–69
82. Kelly SM, Kampe SL. 2004. Microstructural evolution in laser-deposited multilayer Ti6Al-4V build. Part I. Microstructural characterization. *Metall. Mater. Trans. A* 35(June):1861–67
83. Kelly SM, Kampe SL. 2004. Microstructural evolution in laser-deposited multilayer Ti-6Al-4V builds: Part II. Thermal modeling. *Metall. Mater. Trans. A* 35(6):1869–79

84. Buican GR, Oancea G, Lancea C, Pop MA. 2015. Some considerations regarding micro hardness of parts manufactured from 316-L Steel using SLM technology. *Appl. Mech. Mater.* 760:515–20
85. Zhao X, Wei Q, Song B, Liu Y, Luo X, et al. 2015. Fabrication and characterization of AISI 420 stainless steel using selective laser melting. *Mater. Manuf. Process.* 30(11):1283–89
86. Jelis E, Clemente M, Kerwien S, Ravindra NM, Hespos MR. 2015. Metallurgical and mechanical evaluation of 4340 steel produced by direct metal laser sintering. *JOM* 67(3):582–89
87. King WE, Barth HD, Castillo VM, Gallegos GF, Gibbs JW, et al. 2014. Observation of keyhole-mode laser melting in laser powder-bed fusion additive manufacturing. *J. Mater. Process. Technol.* 214(12):2915–25
88. Jägle EA, Choi P. 2014. Precipitation and austenite reversion behavior of a maraging steel produced by selective laser melting. *J. Mater. Res.* 29(17):2072–79
89. Kempen K, Vrancken B, Buls S, Thijs L, Van Humbeeck J, Kruth J-P. 2014. Selective laser melting of crack-free high density M2 high speed steel parts by baseplate preheating. *J. Manuf. Sci. Eng.* 136(6):061026
90. Lebrun T, Tanigaki K, Horikawa K, Kobayashi H. 2014. Strain rate sensitivity and mechanical anisotropy of selective laser melted 17-4 PH stainless steel. *Mech. Eng. J.* 1(5):SMM0049
91. Abele E, Stoffregen HA, Kniepkamp M, Lang S, Hampe M. 2014. Selective laser melting for manufacturing of thin-walled porous elements. *J. Mater. Process. Technol.* 215:114–22
92. Riemer A, Leuders S, Thöne M, Richard HA, Tröster T, Niendorf T. 2014. On the fatigue crack growth behavior in 316L stainless steel manufactured by selective laser melting. *Eng. Fract. Mech.* 120:15–25
93. Tolosa I, Garciandía F, Zubiri F, Zapirain F, Esnaola A. 2010. Study of mechanical properties of AISI 316 stainless steel processed by 'selective laser melting', following different manufacturing strategies. *Int. J. Adv. Manuf. Technol.* 51(5–8):639–47
94. Wanjara P, Brochu M, Jahazi M. 2007. Electron beam freeforming of stainless steel using solid wire feed. *Mater. Des.* 28(8):2278–86
95. Sun G, Zhou R, Lu J, Mazumder J. 2015. Evaluation of defect density, microstructure, residual stress, elastic modulus, hardness and strength of laser-deposited AISI 4340 steel. *Acta Mater.* 84:172–89
96. Colegrove PA, Coules HE, Fairman J, Martina F, Kashoob T, et al. 2013. Microstructure and residual stress improvement in wire and arc additively manufactured parts through high-pressure rolling. *J. Mater. Process. Technol.* 213(10):1782–91
97. You X, Tan Y, Li J, Li P, Dong C, et al. 2015. Effects of solution heat treatment on the microstructure and hardness of Inconel 740 superalloy prepared by electron beam smelting. *J. Alloys Compd.* 638:239–48
98. List FA, Dehoff RR, Lowe LE, Sames WJ. 2014. Properties of Inconel 625 mesh structures grown by electron beam additive manufacturing. *Mater. Sci. Eng. A* 615:191–97
99. Tayon WA, Shenoy RN, Redding MR, Bird RK, Hafley RA. 2014. Correlation between microstructure and mechanical properties in an Inconel 718 deposit produced via electron beam freeform fabrication. *J. Manuf. Sci. Eng.* 136(6):061005
100. Martinez E, Murr LE, Hernandez J, Pan X, Amato K, et al. 2013. Microstructures of niobium components fabricated by electron beam melting. *Metallogr. Microstruct. Anal.* 2(3):183–89
101. Murr LE, Martinez E, Pan XM, Gaytan SM, Castro JA, et al. 2013. Microstructures of Rene 142 nickel-based superalloy fabricated by electron beam melting. *Acta Mater.* 61(11):4289–96
102. Murr LE, Martinez E, Gaytan SM, Ramirez DA, Machado BI, et al. 2011. Microstructural architecture, microstructures, and mechanical properties for a nickel-base superalloy fabricated by electron beam melting. *Metall. Mater. Trans. A* 42(11):3491–508
103. Li S, Wei Q, Shi Y, Zhu Z, Zhang D. 2015. Microstructure characteristics of Inconel 625 superalloy manufactured by selective laser melting. *J. Mater. Sci. Technol.* 31(9):946–52
104. Strößner J, Terock M, Glatzel U. 2015. Mechanical and microstructural investigation of nickel-based superalloy IN718 manufactured by selective laser melting (SLM). *Adv. Eng. Mater.* 17(8):1099–105
105. Scott-Emuakpor O, Schwartz J, George T, Holycross C, Cross C, Slater J. 2015. Bending fatigue life characterisation of direct metal laser sintering nickel alloy 718. *Fatigue Fract. Eng. Mater. Struct.* 38(9):1105–17
106. Harrison NJ, Todd I, Mumtaz K. 2015. Reduction of micro-cracking in nickel superalloys processed by Selective Laser Melting: a fundamental alloy design approach. *Acta Mater.* 94:59–68

107. Kunze K, Etter T, Grässlin J, Shklover V. 2015. Texture, anisotropy in microstructure and mechanical properties of IN738LC alloy processed by selective laser melting (SLM). *Mater. Sci. Eng. A* 620:213–22
108. Carter LN, Martin C, Withers PJ, Attallah MM. 2014. The influence of the laser scan strategy on grain structure and cracking behaviour in SLM powder-bed fabricated nickel superalloy. *J. Alloys Compd.* 615:338–47
109. Kanagarajah P, Brenne F, Niendorf T, Maier HJ. 2013. Inconel 939 processed by selective laser melting: effect of microstructure and temperature on the mechanical properties under static and cyclic loading. *Mater. Sci. Eng. A* 588:188–95
110. Benn RC, Salva RP, Engineering P. 2010. Additively manufactured Inconel alloy 718. In *TMS Superalloy 718 and Derivatives Proceedings*, *7th*, pp. 455–69. Warrendale, PA/Hoboken, NJ: TMS/Wiley
111. Zhang Y-N, Cao X, Wanjara P, Medraj M. 2014. Tensile properties of laser additive manufactured Inconel 718 using filler wire. *J. Mater. Res.* 29(17):2006–20
112. Dehoff RR, Sarosi PM, Collins PC, Fraser HL, Mills MJ. 2003. Microstructural evaluation of LENS$^{TM}$ deposited Nb-Ti-Si-Cr alloys. *MRS Proc.* 753:BB2.6
113. Gu D, Wang H, Dai D, Yuan P, Meiners W, Poprawe R. 2015. Rapid fabrication of Al-based bulk-form nanocomposites with novel reinforcement and enhanced performance by selective laser melting. *Scr. Mater.* 96:25–28
114. Weingarten C, Buchbinder D, Pirch N, Meiners W, Wissenbach K, Poprawe R. 2015. Formation and reduction of hydrogen porosity during selective laser melting of AlSi10Mg. *J. Mater. Process. Technol.* 221:112–20
115. Siddique S, Imran M, Wycisk E, Emmelmann C, Walther F. 2015. Influence of process-induced microstructure and imperfections on mechanical properties of AlSi12 processed by selective laser melting. *J. Mater. Process. Technol.* 221:205–13
116. Yan C, Hao L, Hussein A, Young P, Huang J, Zhu W. 2015. Microstructure and mechanical properties of aluminium alloy cellular lattice structures manufactured by direct metal laser sintering. *Mater. Sci. Eng. A* 628:238–46
117. Olakanmi EO, Cochrane RF, Dalgarno KW. 2015. A review on selective laser sintering/melting (SLS/SLM) of aluminium alloy powders: processing, microstructure, and properties. *Prog. Mater. Sci.* 74:401–77
118. Kempen K, Thijs L, Van Humbeeck J, Kruth J-P. 2015. Processing AlSi10Mg by selective laser melting: parameter optimisation and material characterisation. *Mater. Sci. Technol.* 31(8):917–23
119. Krishnan M, Atzeni E, Canali R, Calignano F, Manfredi D, et al. 2014. On the effect of process parameters on properties of AlSi10Mg parts produced by DMLS. *Rapid Prototyp. J.* 20(6):449–58
120. Rometsch PA, Zhong H, Nairn KM, Jarvis T, Wu X. 2014. Characterization of a laser-fabricated hypereutectic Al-Sc alloy bar. *Scr. Mater.* 87:13–16
121. Li Y, Gu D. 2014. Parametric analysis of thermal behavior during selective laser melting additive manufacturing of aluminum alloy powder. *Mater. Des.* 63:856–67
122. Mertens R, Clijsters S, Kempen K, Kruth J-P. 2014. Optimization of scan strategies in selective laser melting of aluminum parts with downfacing areas. *J. Manuf. Sci. Eng.* 136(6):06 1012
123. Aboulkhair NT, Everitt NM, Ashcroft I, Tuck C. 2014. Reducing porosity in AlSi10Mg parts processed by selective laser melting. *Addit. Manuf.* 1–4:77–86
124. Rosenthal I, Stern A, Frage N. 2014. Microstructure and mechanical properties of AlSi10Mg parts produced by the laser beam additive manufacturing (AM) technology. *Metallogr. Microstruct. Anal.* 3(6):448–53
125. Taminger K, Hafley R. 2003. Electron beam freeform fabrication: a rapid metal deposition process. In *Proc. Annu. Automot. Compos. Conf.*, *3rd*, pp. 9–10
126. Li X, Reynolds AP, Cong B, Ding J, Williams S. 2015. Production and properties of a wire-arc additive manufacturing part made with friction extruded wire. In *TMS Proceedings*, pp. 445–52. Warrendale, PA/Hoboken, NJ: TMS/Wiley
127. Gu J, Cong B, Ding J, Williams SW, Zhai Y. 2014. Wire+arc additive manufacturing of aluminum. In *Solid Freeform Fabrication Proceedings*, pp. 451–58. Austin: Univ. Tex.

128. Fujieda T, Shiratori H, Kuwabara K, Kato T, Yamanaka K, et al. 2015. First demonstration of promising selective electron beam melting method for utilizing high-entropy alloys as engineering materials. *Mater. Lett.* 159(15):12–15
129. Brif Y, Thomas M, Todd I. 2015. The use of high-entropy alloys in additive manufacturing. *Scr. Mater.* 99:93–96
130. ISO/ASTM. 2013. *Standard terminology for additive manufacturing-coordinate systems and test methodologies*. ASTM/ISO Stand. 52921
131. ASTM. 2015. *Guide for orientation and location dependence mechanical properties for metal additive manufacturing*. ASTM Work Item WK49229
132. Moylan S, Land J, Possolo A. 2015. Additive manufacturing round robin protocols: a pilot study. In *Solid Freeform Fabrication Proceedings*, pp. 1504–12. Austin: Univ. Tex.
133. Moylan S, Slotwinski J. 2014. Assessment of guidelines for conducting round robin studies in additive manufacturing. In *Proceedings of ASPE Spring Topical Meeting—Dimensional Accuracy and Surface Finish in Additive Manufacturing*, Vol. 57, pp. 82–85. Berkeley, CA: NIST
134. Gockel J, Beuth J, Taminger K. 2014. Integrated control of solidification microstructure and melt pool dimensions in electron beam wire feed additive manufacturing of Ti-6Al-4V. *Addit. Manuf.* 1–4:119–26
135. Beuth J, Fox J, Gockel J, Montgomery C, Yang R, et al. 2013. Process mapping for qualification across multiple direct metal additive manufacturing processes. In *Solid Freeform Fabrication Proceedings*, pp. 655–65. Austin: Univ. Tex.
136. Gockel J, Beuth J. 2013. Understanding Ti-6Al-4V microstructure control in additive manufacturing via process maps. In *Solid Freeform Fabrication Proceedings*, pp. 666–74. Austin: Univ. Tex.
137. Nassar AR, Keist JS, Reutzel EW, Spurgeon TJ. 2015. Intra-layer closed-loop control of build plan during directed energy additive manufacturing of Ti-6Al-4V. *Addit. Manuf.* 6:39–52
138. Soylemez E, Beuth JL, Taminger K. 2010. Controlling melt pool dimensions over a wide range of material deposition rates in electron beam additive manufacturing. In *Solid Freeform Fabrication Proceedings*, pp. 571–82. Austin: Univ. Tex.
139. Montgomery C, Beuth J, Sheridan L, Klingbeil N. 2015. Process mapping of Inconel 625 in laser powder bed additive manufacturing. In *Solid Freeform Fabrication Proceedings*, pp. 1195–204. Austin: Univ. Tex.
140. Seifi M, Christiansen D, Beuth JL, Harrysson O, Lewandowski JJ. 2016. Process mapping, fracture and fatigue behavior of Ti-6Al-4V produced by EBM additive manufacturing. In *Proceedings of World Conference on Titanium, 13th*, pp. 1373–77. Warrendale, PA/Hoboken, NJ: TMS/Wiley
141. Greitemeier D, Dalle Donne C, Syassen F, Eufinger J, Melz T. 2016. Effect of surface roughness on fatigue performance of additive manufactured Ti-6Al-4V. *Mater. Sci. Technol.* In press
142. Edwards P, O'Conner A, Ramulu M. 2013. Electron beam additive manufacturing of titanium components: properties and performance. *J. Manuf. Sci. Eng.* 135(6):061016
143. Tan X, Kok Y, Tan YJ, Descoins M, Mangelinck D, et al. 2015. Graded microstructure and mechanical properties of additive manufactured Ti-6Al-4V via electron beam melting. *Acta Mater.* 97:1–16
144. Rodriguez OL, Allison PG, Whittington WR, Francis DK, Rivera OG, et al. 2015. Dynamic tensile behavior of electron beam additive manufactured Ti-6Al-4V. *Mater. Sci. Eng. A* 641:323–27
145. Hrabe N, Quinn T. 2013. Effects of processing on microstructure and mechanical properties of a titanium alloy (Ti-6Al-4V) fabricated using electron beam melting (EBM). Part 2. Energy input, orientation, and location. *Mater. Sci. Eng. A* 573:271–77
146. Murr LE, Esquivel EV, Quinones SA, Gaytan SM, Lopez MI, et al. 2009. Microstructures and mechanical properties of electron beam–rapid manufactured Ti-6Al-4V biomedical prototypes compared to wrought Ti-6Al-4V. *Mater. Charact.* 60(2):96–105
147. McLouth T, Chang Y, Wooten J, Yang J. 2015. The effects of electron beam melting on the microstructure and mechanical properties of Ti-6Al-4V and γ-TiAl. *Microsc. Microanal.* 21(588):1177–78
148. Gong H, Rafi K, Gu H, Janaki Ram GD, Starr T, Stucker B. 2015. Influence of defects on mechanical properties of Ti-6Al-4V components produced by selective laser melting and electron beam melting. *Mater. Des.* 86:545–54
149. Morgan L, Lindhe U, Harrysson O. 2003. Rapid manufacturing with electron beam melting (EBM)—a manufacturing revolution? In *Solid Freeform Fabrication Proceedings*, pp. 433–38. Austin: Univ. Tex.

150. Rekedal KD, Liu D. 2015. Fatigue life of selective laser melted and hot isostatically pressed Ti-6Al-4V absent of surface machining. Presented at *AIAA/ASCE/AHS/ASC Structures, Structural Dynamics, and Materials Conference, 56th*
151. Cain V, Thijs L, Van Humbeeck J, Van Hooreweder B, Knutsen R. 2015. Crack propagation and fracture toughness of Ti-6Al-4V alloy produced by selective laser melting. *Addit. Manuf.* 5(1):68–76
152. Kasperovich G, Hausmann J. 2015. Improvement of fatigue resistance and ductility of TiAl6V4 processed by selective laser melting. *J. Mater. Process. Technol.* 220:202–14
153. Edwards P, Ramulu M. 2014. Fatigue performance evaluation of selective laser melted Ti-6Al-4V. *Mater. Sci. Eng. A* 598:327–37
154. Leuders S, Lieneke T, Lammers S, Tröster T, Niendorf T. 2014. On the fatigue properties of metals manufactured by selective laser melting—the role of ductility. *J. Mater. Res.* 29(17):1911–19
155. Simonelli M, Tse YY, Tuck C. 2014. Effect of the build orientation on the mechanical properties and fracture modes of SLM Ti-6Al-4V. *Mater. Sci. Eng. A* 616(10):1–11
156. Vrancken B, Thijs L, Kruth J-P, Van Humbeeck J. 2012. Heat treatment of Ti-6Al-4V produced by Selective Laser Melting: microstructure and mechanical properties. *J. Alloys Compd.* 541:177–85
157. Murr LE, Quinones SA, Gaytan SM, Lopez MI, Rodela A, et al. 2009. Microstructure and mechanical behavior of Ti-6Al-4V produced by rapid-layer manufacturing, for biomedical applications. *J. Mech. Behav. Biomed. Mater.* 2(1):20–32
158. Vilaro T, Colin C, Bartout JD. 2011. As-fabricated and heat-treated microstructures of the Ti-6Al-4V alloy processed by selective laser melting. *Metall. Mater. Trans. A* 42(10):3190–99
159. Vandenbroucke B, Kruth JP. 2007. Selective laser melting of biocompatible metals for rapid manufacturing of medical parts. *Rapid Prototyp. J.* 13(4):196–203
160. Mertens A, Reginster S, Paydas H, Contrepois Q, Dormal T, et al. 2014. Mechanical properties of alloy Ti-6Al-4V and of stainless steel 316L processed by selective laser melting: influence of out-of-equilibrium microstructures. *Powder Metall.* 57(3):184–89
161. Hollander DA, von Walter M, Wirtz T, Sellei R, Schmidt-Rohlfing B, et al. 2006. Structural, mechanical and in vitro characterization of individually structured Ti-6Al-4V produced by direct laser forming. *Biomaterials* 27(7):955–63
162. Qiu C, Adkins NJE, Attallah MM. 2013. Microstructure and tensile properties of selectively laser-melted and of HIPed laser-melted Ti-6Al-4V. *Mater. Sci. Eng. A* 578:230–39
163. Yu J, Rombouts M, Maes G, Motmans F. 2012. Material properties of Ti-6Al-4V parts produced by laser metal deposition. *Phys. Procedia* 39:416–24
164. Zhang S, Lin X, Chen J, Huang W. 2009. Heat-treated microstructure and mechanical properties of laser solid forming Ti-6Al-4V alloy. *Rare Met.* 28(6):537–44
165. Alcisto J, Enriquez A, Garcia H, Hinkson S, Steelman T, et al. 2011. Tensile properties and microstructures of laser-formed Ti-6Al-4V. *J. Mater. Eng. Perform.* 20(2):203–12
166. Dinda GP, Song L, Mazumder J. 2008. Fabrication of Ti-6Al-4V scaffolds by direct metal deposition. *Metall. Mater. Trans. A* 39(12):2914–22
167. Zhai Y, Galarraga H, Lados DA. 2015. Microstructure evolution, tensile properties, fatigue damage mechanisms in Ti-6Al-4V alloys fabricated by two additive manufacturing techniques. *Procedia Eng.* 114:658–66
168. Arcella FG, Froes FH. 2000. Producing titanium aerospace components from powder using laser forming. *JOM* 52(5):28–30
169. Lewis GK, Schlienger E. 2000. Practical considerations and capabilities for laser assisted direct metal deposition. *Mater. Des.* 21(4):417–23
170. Griffith ML, Ensz MT, Puskar JD, Robino CV, Brooks JA, et al. 2000. Understanding the microstructure and properties of components fabricated by Laser Engineered Net Shaping (LENS). *MRS Proc.* 625:9; doi: 10.1557/PROC-625-9
171. Löber L, Schimansky FP, Kühn U, Pyczak F, Eckert J. 2014. Selective laser melting of a beta-solidifying TNM-B1 titanium aluminide alloy. *J. Mater. Process. Technol.* 214(9):1852–60
172. Löber L, Biamino S, Ackelid U, Sabbadini S, Epicoco P, et al. 2011. Comparison of selective laser and electron beam melted titanium aluminides. In *Solid Freeform Fabrication Proceedings*, pp. 547–56. Austin: Univ. Tex.

173. Spierings AB, Starr TL, Ag I. 2013. Fatigue performance of additive manufactured metallic parts. *Rapid Prototyp. J.* 19(2):88–94
174. Sercombe TB, Li X. 2016. Selective laser melting of aluminium and aluminium metal matrix composites: review. *Mater. Technol.* In press
175. Wang XJ, Zhang LC, Fang MH, Sercombe TB. 2014. The effect of atmosphere on the structure and properties of a selective laser melted Al-12Si alloy. *Mater. Sci. Eng. A* 597:370–75
176. Li XP, Wang XJ, Saunders M, Suvorova A, Zhang LC, et al. 2015. A selective laser melting and solution heat treatment refined Al-12Si alloy with a controllable ultrafine eutectic microstructure and 25% tensile ductility. *Acta Mater.* 95:74–82
177. Read N, Wang W, Essa K, Attallah MM. 2015. Selective laser melting of AlSi10Mg alloy: process optimisation and mechanical properties development. *Mater. Des.* 65:417–24
178. Manfredi D, Calignano F, Krishnan M, Canali R, Ambrosio EP, Atzeni E. 2013. From powders to dense metal parts: characterization of a commercial AlSiMg alloy processed through direct metal laser sintering. *Materials* 6(3):856–69
179. Kempen K, Thijs L, Van Humbeeck J, Kruth J-P. 2012. Mechanical properties of AlSi10Mg produced by selective laser melting. *Phys. Procedia* 39:439–46
180. Song C, Yang Y, Wang Y, Wang D, Yu J. 2014. Research on rapid manufacturing of CoCrMo alloy femoral component based on selective laser melting. *Int. J. Adv. Manuf. Technol.* 75(1–4):445–53
181. Kircher R, Christensen A, Wurth K. 2009. Electron Beam Melted (EBM) Co-Cr-Mo alloy for orthopaedic implant applications. In *Solid Freeform Fabrication Proceedings*, pp. 428–36. Austin: Univ. Tex.
182. Tarasova TV, Nazarov AP, Prokof'ev MV. 2015. Effect of the regimes of selective laser melting on the structure and physicomechanical properties of cobalt-base superalloys. *Phys. Met. Metallogr.* 116(6):601–5
183. Terrazas CA, Mireles J, Gaytan SM, Morton PA, Hinojos A, et al. 2016. Fabrication and characterization of high-purity niobium using electron beam melting additive manufacturing technology. *Int. J. Adv. Manuf. Technol.* In press
184. Wei K, Gao M, Wang Z, Zeng X. 2014. Effect of energy input on formability, microstructure and mechanical properties of selective laser melted AZ91D magnesium alloy. *Mater. Sci. Eng. A* 611:212–22
185. Ma Y, Cuiuri D, Hoye N, Li H, Pan Z. 2015. The effect of location on the microstructure and mechanical properties of titanium aluminides produced by additive layer manufacturing using in-situ alloying and gas tungsten arc welding. *Mater. Sci. Eng. A* 631:230–40
186. Baufeld B. 2012. Mechanical properties of INCONEL 718 parts manufactured by shaped metal deposition (SMD). *J. Mater. Eng. Perform.* 21(7):1416–21
187. Blackwell PL. 2005. The mechanical and microstructural characteristics of laser-deposited IN718. *J. Mater. Process. Technol.* 170(1–2):240–46
188. Zhao X, Chen J, Lin X, Huang W. 2008. Study on microstructure and mechanical properties of laser rapid forming Inconel 718. *Mater. Sci. Eng. A* 478(1–2):119–24
189. Bird RK, Hibberd J. 2009. *Tensile properties and microstructure of Inconel 718 fabricated with electron beam freeform fabrication (EBF$^3$)*. Tech. Rep., NASA
190. Qi H, Azer M, Ritter A. 2009. Studies of standard heat treatment effects on microstructure and mechanical properties of laser net shape manufactured INCONEL 718. *Metall. Mater. Trans. A* 40(10):2410–22
191. Cao X, Rivaux B, Jahazi M, Cuddy J, Birur A. 2009. Effect of pre- and post-weld heat treatment on metallurgical and tensile properties of Inconel 718 alloy butt joints welded using 4kW Nd:YAG laser. *J. Mater. Sci.* 44(17):4557–71
192. Edwards P, Ramulu M. 2015. Effect of build direction on the fracture toughness and fatigue crack growth in selective laser melted Ti-6Al-4V. *Fatigue Fract. Eng. Mater. Struct.* 38(10):1228–36
193. Van Hooreweder B, Moens D, Boonen R, Kruth J-P, Sas P. 2012. Analysis of fracture toughness and crack propagation of Ti-6Al-4V produced by selective laser melting. *Adv. Eng. Mater.* 14(1–2):92–97
194. Becker TH, Beck M, Scheffer C. 2015. Microstructure and mechanical properties of direct metal laser sintered Ti-6Al-4V. *S. Afr. J. Ind. J.* 26:1–10
195. Svensson M. 2009. Ti6Al4V manufactured with electron beam melting (EBM): mechanical and chemical properties. In *Proceedings from the Materials & Processes for Medical Devices Conference*, pp. 189–94. Novelty, OH: ASM Int.

196. Boyer R, Welsch G, Collings EW. 1994. *Materials Properties Handbook: Titanium Alloys*. Novelty, OH: ASM Int.
197. Seifi M, Salem A, Satko D, Shaffer J, Lewandowski JJ. 2016. Fracture resistance and fatigue behavior of Ti-6Al-4V additively manufactured by electron beam melting (EBM): role of microstructure heterogeneity, defect distribution and post-processing. *Int. J. Fatigue*. In press
198. Seifi M, Ghamarian I, Samimi P, Collins PC, Lewandowski JJ. 2016. Microstructure and mechanical properties of Ti-48Al-2Cr-2Nb manufactured via electron beam melting. In *Proceedings of World Conference on Titanium*, *13th*, pp. 1317–22. Warrendale, PA/Hoboken, NJ: TMS/Wiley
199. Seifi M, Salem A, Satko D, Ackelid U, Lewandowski JJ. 2016. Effects of microstructural heterogeneity and post-processing on mechanical properties of Ti-48Al-2Cr-2Nb additively manufactured by electron beam melting (EBM). *Intermetallics*. Under review
200. Dahar MS, Seifi SM, Bewlay BP, Lewandowski JJ. 2015. Effects of test orientation on fracture and fatigue crack growth behavior of third generation as-cast Ti-48Al-2Nb-2Cr. *Intermetallics* 57:73–82
201. Li P, Warner DH, Fatemi A, Phan N. 2015. Critical assessment of the fatigue performance of additively manufactured Ti-6Al-4V and perspective for future research. *Int. J. Fatigue* 85:130–43
202. Fodran E, Walker K. 2015. *Surface finish enhancement for the electron beam direct digital manufacturing of Ti-6Al-4V alloy structural components*. Tech. Rep., Armament Research, Development and Engineering Center, Weapons Software Engineering Center, Benét Lab.
203. Seifi M, Lewandowski JJ. 2016. Microstructure and mechanical properties of additively manufactured alloys. *Prog. Mater. Sci.* In preparation
204. Filippini M, Beretta S, Içöz C, Patriarca L. 2015. Effect of the microstructure on the fatigue strength of a TiAl intermetallic alloy produced by additive manufacturing. *Mater. Res. Soc. Symp. Proc.* 1:3–8
205. McLouth T, Chang Y, Wooten J, Yang J. 2015. The effects of electron beam melting on the microstructure and mechanical properties of Ti-6Al-4V and γ-TiAl. *Microsc. Microanal.* 21(588):1177–78
206. Seikh A, Mohammad A, Sherif E-S, Al-Ahmari A. 2015. Corrosion behavior in 3.5% NaCl solutions of γ-TiAl processed by electron beam melting process. *Metals* 5(4):2289–302
207. Tang HP, Yang GY, Jia WP, He WW, Lu SL, Qian M. 2015. Additive manufacturing of a high niobium-containing titanium aluminide alloy by selective electron beam melting. *Mater. Sci. Eng. A* 636:103–7
208. Biamino S, Klöden B, Weißgärber T, Kieback B, Ackelid U. 2014. Titanium aluminides for automotive applications processed by electron beam melting. In *Proceedings of Metal Powder Industries Federation (MPIF)*, pp. 96–103. Princeton, NJ: MPIF
209. Filippini M, Beretta S, Patriarca L, Sabbadini S. 2014. Effect of the microstructure on the deformation and fatigue damage in a gamma TiAl produced by additive manufacturing. In *TMS Proceedings*, pp. 189–93. Warrendale, PA/Hoboken, NJ: TMS/Wiley
210. Ge W, Guo C, Lin F. 2014. Effect of process parameters on microstructure of TiAl alloy produced by electron beam selective melting. *Procedia Eng.* 81:1192–97
211. Ge W, Lin F, Guo C. 2014. The effect of scan pattern on microstructure evolution and mechanical properties in electron beam melting Ti47Al2Cr2Nb. In *Solid Freeform Fabrication Proceedings*, pp. 501–13. Austin: Univ. Tex.
212. Schwerdtfeger J, Körner C. 2014. Selective electron beam melting of Ti-48Al-2Nb-2Cr: microstructure and aluminium loss. *Intermetallics* 49:29–35
213. Filippini M, Beretta S, Patriarca L, Pasquero G, Sabbadini S. 2012. Fatigue sensitivity to small defects of a gamma–titanium–aluminide alloy. *J. ASTM Int.* 9(5):104293
214. Terner M, Biamino S, Ugues D, Sabbadini S, Fino P, et al. 2013. Phase transitions assessment on γ-TiAl by thermo mechanical analysis. *Intermetallics* 37:7–10
215. Hernandez J, Murr LE, Gaytan SM, Martinez E, Medina F, Wicker RB. 2012. Microstructures for two-phase gamma titanium aluminide fabricated by electron beam melting. *Metallogr. Microstruct. Anal.* 1(1):14–27
216. Biamino S, Penna A, Ackelid U, Sabbadini S, Tassa O, et al. 2011. Electron beam melting of Ti–48Al–2Cr–2Nb alloy: microstructure and mechanical properties investigation. *Intermetallics* 19(6):776–81
217. Filippini M, Beretta S, Patriarca L, Pasquero G, Sabbadini S. 2011. Defect tolerance of a gamma titanium aluminide alloy. *Procedia Eng.* 10:3677–82

218. Franzen SF, Karlsson J, Dehoff R, Ackelid U, Rios O, et al. 2011. Microstructural properties of gamma titanium aluminide manufactured by electron beam melting. In *TMS Proceedings*, pp. 455–62. Warrendale, PA/Hoboken, NJ: TMS/Wiley
219. Murr LE, Gaytan SM, Ceylan A, Martinez E, Martinez JL, et al. 2010. Characterization of titanium aluminide alloy components fabricated by additive manufacturing using electron beam melting. *Acta Mater.* 58(5):1887–94
220. Patriarca L. 2010. Fatigue crack growth of a gamma titanium aluminide alloy. In *Youth Symposium on Experimental Solid Mechanics, 9th*, pp. 36–39
221. Sabbadini S, Tassa O, Gennaro P, Ackelid U. 2010. Additive manufacturing of gamma titanium aluminide parts by electron beam melting. In *TMS Proceedings*, pp. 267–74. Warrendale, PA/Hoboken, NJ: TMS/Wiley
222. Cormier D, Harrysson O, Mahale T, West H. 2007. Freeform fabrication of titanium aluminide via electron beam melting using prealloyed and blended powders. *Res. Lett. Mater. Sci.* 2007:1–4
223. Li W, Liu J, Wen W, Wei Q, Yan C, Shi Y. 2016. Crystal orientation, crystallographic texture and phase evolution in the Ti–45Al–2Cr–5Nb alloy processed by selective laser melting. *Mater. Charact.* 113:125–33
224. Gussone J, Hagedorn Y-C, Gherekhloo H, Kasperovich G, Merzouk T, Hausmann J. 2015. Microstructure of $\gamma$-titanium aluminide processed by selected laser melting at elevated temperatures. *Intermetallics* 66:133–40
225. Yadollahi A, Shamsaei N, Thompson SM, Seely DW. 2015. Effects of process time interval and heat treatment on the mechanical and microstructural properties of direct laser deposited 316L stainless steel. *Mater. Sci. Eng. A* 644:171–83
226. Sterling A, Torries B, Shamsaei N, Thompson SM, Seely DW. 2016. Fatigue behavior and failure mechanisms of direct laser deposited Ti-6Al-4V. *Mater. Sci. Eng. A* 655:100–12